ACS OMEGA

http://pubs.acs.org/journal/acsodf

Article

Unveiling Structural Diversity of Uranyl Compounds of Aprotic 4,4′-Bipyridine *N,N′*-Dioxide Bearing O-Donors

Jing-yang Wang, Lei Mei,* Yang Liu, Qiu-yan Jin, Kong-qiu Hu, Ji-pan Yu, Cai-shan Jiao, Meng Zhang,* and Wei-qun Shi

Cite This: *ACS Omega* 2023, 8, 8894−8909

Read Online

ACCESS | Metrics & More | Article Recommendations | Supporting Information

ABSTRACT: As an aprotic O-donor ligand, 4,4′-bipyridine *N,N′*-dioxide (DPO) shows good potential for the preparation of uranyl coordination compounds. In this work, by regulating reactant compositions and synthesis conditions, diverse coordination assembly between uranyl and DPO under different reaction conditions was achieved in the presence of other coexisting O-donors. A total of ten uranyl-DPO compounds, U-DPO-1 to U-DPO-10, have been synthesized by evaporation or hydro/solvothermal treatment, and the possible competition and cooperation of DPO with other O-donors for the formation of these uranyl-DPO compounds are discussed. Starting with an aqueous solution of uranyl nitrate, it is found that an anionic nitrate or hydroxyl group is involved in the coordination sphere of uranyl in U-DPO-1 ($(UO_2)(NO_3)_2(H_2O)_2\cdot(DPO)$), U-DPO-2 ($(UO_2)(NO_3)_2(DPO)$), and U-DPO-3 ($(UO_2)(DPO)(\mu_2\text{-}OH)_2$), where DPO takes three different kinds of coordination modes, i.e. uncoordinated, monodentate, and biconnected. The utilization of $UO_2(CF_3SO_3)_2$ in acetonitrile, instead of an aqueous solution of uranyl nitrate, precludes the participation of nitrate and hydroxyl, and ensures the engagement of DPO ligands (4−5 DPO ligands for each uranyl) in a uranyl coordination sphere of U-DPO-4 ($[(UO_2)(CF_3SO_3)(DPO)_2](CF_3SO_3)$), U-DPO-5 ($[UO_2(H_2O)(DPO)_2](CF_3SO_3)_2$) and U-DPO-6 ($[(UO_2)(DPO)_{2.5}](CF_3SO_3)_2$). Moreover, when combined with anionic carboxylate ligands, terephthalic acid (H_2TPA), isophthalic acid (H_2IPA), and succinic acid (H_2SA), DPO works well with them to produce four mixed-ligand uranyl compounds with similar structures of two-dimensional (2D) networks or three-dimensional (3D) frameworks, U-DPO-7 ($(UO_2)(TPA)(DPO)$), U-DPO-8 ($(UO_2)_2(DPO)(IPA)_2\cdot 0.5H_2O$), U-DPO-9 ($(UO_2)(SA)(DPO)\cdot H_2O$), and U-DPO-10 ($(UO_2)_2(\mu_2\text{-}OH)(SA)_{1.5}(DPO)$). Density functional theory (DFT) calculations conducted to probe the bonding features between uranyl ions and different O-donor ligands show that the bonding ability of DPO is better than that of anionic $CF_3SO_3^-$, nitrate, and a neutral H_2O molecule and comparable to that of an anionic carboxylate group. Characterization of physicochemical properties of U-DPO-7 and U-DPO-10 with high phase purity including infrared (IR) spectroscopy, thermogravimetric analysis (TGA), and luminescence properties is also provided.

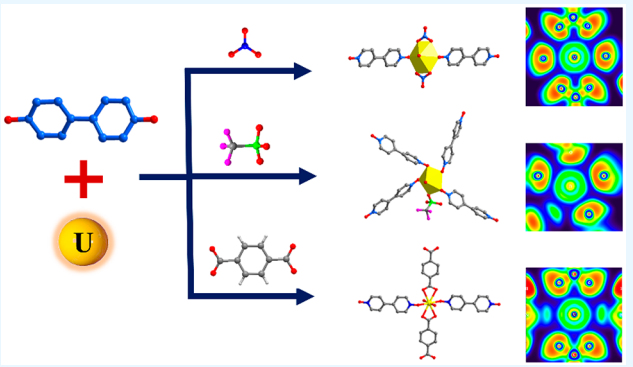

INTRODUCTION

Coordination polymers (CPs)[1−4] have received extensive attention due to their adjustable architectures and topologies[5−8] and potential applications in various fields, such as dye adsorption,[9−13] catalysis,[14−17] nuclide removal,[18−21] luminescence sensing,[22−24] and so forth. Compared with the rapidly increasing number of CPs based on transition metal and lanthanide nodes,[25−27] studies on actinide-involving CPs are relatively insufficient due to their intrinsic radioactivity and less availability. Actinides play an important role in the development of nuclear industries, e.g., actinide-related nuclides being taken as the focus of attention in the process of spent fuel reprocessing. The study of actinide-based CPs can inspire new strategies for spent nuclear fuel management[28,29] and also benefit the exploration of actinide hybrid materials and their utilization.[30,31] Moreover, stemming from their characteristic 5f electron orbitals and large ionic radii,[32−34] actinide ions show intriguing bonding features and high coordination numbers in actinide compounds, which distinguish them from transition metals or rare earth ions.

As a representative, uranium-related CPs account for the vast majority of actinide-based materials. In these compounds, uranyl (UO_2^{2+}) cation with a special linear structure is frequently

Received: January 31, 2023
Accepted: February 14, 2023
Published: February 24, 2023

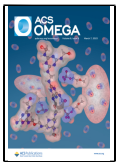

https://doi.org/10.1021/acsomega.3c00640
ACS Omega 2023, 8, 8894−8909

Scheme 1. Comparison of Carboxylic Acids and Phosphonic Acids with Aprotic Ligands in Terms of the Need for Deprotonation Prior to Uranyl Coordination: (a) Carboxylic Acids and Phosphonic Acids That Need to Deprotonate; (b) N-Oxide That Is Deprotonation-Free.

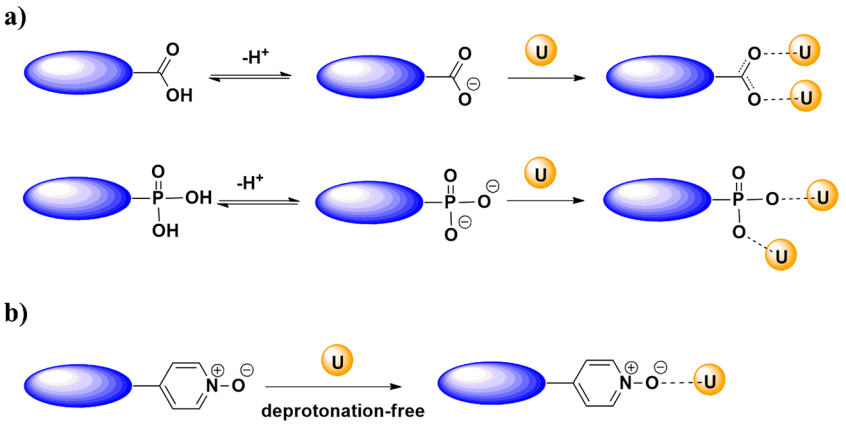

employed, in which, since the preoccupancy of axial oxygen atoms, the exogenous ligands coordinate with a uranium center around its equatorial plane, resulting in tetragonal, pentagonal, and hexagonal bipyramidal geometries.[35] Besides, the hydrolysis of uranyl cations[32,36] and the variety of organic linkers help to achieve rich combinations of topologies in relevant uranyl coordination polymers (UCPs) with zero-dimensional clusters/cages, one-dimensional (1D) chains, two-dimensional (2D) networks, and three-dimensional (3D) frameworks.[37−41] The continuous developments of UCPs can not only provide a better knowledge of coordination assembly[42] and selective recognition[43,44] of uranyl using a portfolio of elegantly selected organic ligands with different donor atoms, molecular geometries, and coordination patterns but also help to put forward and identify new functionality that is unique to actinide-based materials closely related to 5f orbitals or intrinsic radioactivity.[45−48] Up to now, a large number of organic ligands containing N- and O-donor atoms[29,49−51] have been designed for efficient coordination of uranyl cation, which subsequently provide valuable hints to the synthesis of various uranyl−organic hybrid materials. For instance, carboxylic ligands,[30,31,39,40] of which each carboxyl group bears two potential oxygen donors, realize the high-efficiency coordination with uranium cations and thus serve as the most employed organic linkers in UCPs reported so far,[39,52] even in those heterometallic analogues based on functional heterocyclic pyridine backbones.[40,53−55] Similarly, phosphonates or organophosphonic acid compounds represent another important class of uranyl ligands for the construction of UCPs.[41] However, the necessity of deprotonation before complexation with a metal ion makes these organic acids pH sensitive and easily affected by the acidity of the solvent environment. Compared to carboxylates and phosphonates, organic ligands with aprotic O-donors, such as amides, ethers, or N-oxides, are less pH sensitive and free of deprotonation before metal coordination (Scheme 1).The attribute of this kind of ligand being inert to acids and bases has been utilized in metal complexation and separation.[44,49,50] Recently, 4,4′-bipyridine *N*,*N*′-dioxide (DPO), an aprotic oxygen-donor ligand, has been employed as building structures to prepare UCPs with varying dimensionalities,[44,56−60] among which this bidentate ligand with a single O-donor at each end works together with other O-donors or N-donors from anions and auxiliary ligands added when coordinating to a uranyl node. The pioneering exploration of DPO-based uranyl compounds demonstrates the feasibility of such an aprotic ligand for the preparation of UCPs and inspires further research on UCPs based on this aprotic ligand.

In this work, by regulating compositions of the reactants and synthesis methods, the coordination assembly between uranyl and DPO under different reaction conditions is investigated comprehensively. A total of ten uranyl-DPO compounds (namely, U-DPO-*n*, *n* = 1−10) were synthesized through different synthesis procedures. The coordination behavior of DPO with uranyl is evaluated by an intensive analysis of bonding features and a direct comparison with other ligands involved, including solvent molecules, counterions, and other auxiliary ligands added. The results show that, together with solvent molecules, anions, and auxiliary ligands, crystal structures of as-synthesized uranyl-DPO products continuously evolve with the change of experimental conditions. To get a deep insight into the differences of coordinating groups in the coordination ability of uranyl, the bonding nature of U−O bonds (U−O(DPO)) between DPO ligands and uranium compared to other U−O bonds including those of uranium with carboxyl groups (U−O(COO^-)), nitrate (U−O(NO_3^-)), sulfonate (U−O($CF_3SO_3^-$)), and water (U−O(H_2O)) were analyzed by theoretical calculations and discussed. Moreover, physicochemical characterization of two uranyl compounds with high phase purity (UPO-7 and UPO-10) out of these uranyl-DPO compounds is also provided.

EXPERIMENTAL SECTION

Materials and Methods. *Caution! Although uranyl nitrate hexahydrate $UO_2(NO_3)_2{\cdot}6H_2O$ was under a laboratory standard, suitable methods and effective precautions should be followed to handle the radioactive and chemically toxic substances.* To facilitate the assembly in organic solvent, $UO_2(NO_3)_2{\cdot}6H_2O$ was transformed into $UO_2(CF_3SO_3)_2$ by treatment with triflic acid under high temperature, and the as-synthesized $UO_2(CF_3SO_3)_2$ was further dissolved in acetonitrile (CH_3CN) to afford a 0.1 M stock solution (see the Supporting Information for a detailed synthetic protocol).[61] 4,4′-Bipyridine-*N*,*N*′-dioxide (DPO) was synthesized according to reported methods,[62,63] and the synthesis details and characterization can be seen in the Supporting Information. All the other reagents are commercially available and used without further purification.

Powder X-ray diffraction (PXRD) characterization was conducted on a Bruker D8 Advance diffractometer equipped with a Cu Kα radiation source (λ = 1.5406 Å). 2θ scanning

https://doi.org/10.1021/acsomega.3c00640
ACS Omega 2023, 8, 8894−8909

covers the range of 5−40° with a step size of 0.02°. Thermogravimetric analysis (TGA) was measured within a temperature range from 25 to 800 °C in air atmosphere using a TA Q500 analyzer with a heating rate of 5 °C/min. The Fourier transform infrared (FT-IR) spectra were obtained from a Bruker Tensor 27 spectrometer using KBr pellets as the matrix, and the vibration peaks located in the range of 4000−400 cm^{-1} were recorded. Fluorescence spectra were measured on a Hitachi F-4600 fluorescence spectrophotometer with an excitation wavelength of 420 nm that is often used for uranyl compounds.

Synthetic Procedures. Uranyl sources with different anions (nitrate or triflate) that are dissolved in suitable solvents such as water or acetonitrile were used. Additional organic carboxylic acids with different structural flexibility, including terephthalic acid (H_2TPA), isophthalic acid (H_2IPA), malonic acid (H_2MA), and succinic acid (H_2SA), were also added as second ligands. All the uranyl compounds reported in this work were synthesized through evaporation or hydrothermal/solvothermal methods, during which different solvents (water or acetonitrile), sources of uranyl cations, and auxiliary ligands were employed as planned. The synthetic conditions are listed in Table 1. Detailed synthetic protocols can been seen in the Supporting Information.

Crystallography. X-ray single crystal structure determination for all these ten uranyl compounds from U-DPO-1 to U-DOP-10 were conducted on a Bruker D8 VENTURE X-ray CMOS diffractometer with a Mo Kα X-ray source (λ = 0.71073 Å) or a Cu Kα X-ray source (λ = 1.54184 Å) at near room temperature. Data frames were collected and processed using APEX 3. The proposed crystal structures were solved by means of direct methods *SHELXT 2014*[64] and refined with full-matrix least-squares by using the SHELXL program.[64,65] The crystal data of all the compounds are given in Table 2. Since only a small size of crystal samples can be obtained even after optimizing synthesis conditions, the R_{int} values for diffraction data of U-DPO-5 and U-DPO-10 are slightly large but seem to have no significant effect on the validation of final molecular structures. All non-hydrogen atoms of these ten compounds were refined with anisotropic displacement parameters. The carbon-bound hydrogen atoms were placed at calculated positions and treated as riding atoms with an isotropic displacement parameter equal to 1.2 times that of the parent carbon atom. Crystallographic data in this work have been deposited with Cambridge Crystallographic Data Centre, and the CCDC numbers are 2153502 (U-DPO-1), 2153503 (U-DPO-2), 2153504 (U-DPO-3), 2153505 (U-DPO-4), 2153506 (U-DPO-5), 2153507 (U-DPO-6), 2153508 (U-DPO-7), 2153509 (U-DPO-8), 2153510 (U-DPO-9), and 2153511 (U-DPO-10) respectively.

Theoretical Calculations. In order to gain a deeper understanding of the bonding features of different oxygen donor atoms (U−O(DPO), U−O(H_2O), U−O(NO_3^-), U−O($CF_3SO_3^-$), and U−O(COO^-)) with uranyl ions and make a comparison between them, simplified model structures that represent coordination spheres of uranyl in these uranyl−DPO compounds are extracted from their corresponding crystal structures and subject to optimization and analyses by means of scalar relativistic density functional theory (DFT). All the bond order computing of U−O bonds adopted the ADF 2013.01 package[66] at the BP86/TZ2P level of theory. The zero-order regular approximation (ZORA) method[67] was used to consider the scalar relativistic effects of uranium. The quantum theory of atoms in molecules (QTAIM)[68] and electron localization

Table 1. Synthetic Information for All the Uranyl-DPO Compounds Ranging from U-DPO-1 to U-DPO-10

	U-DPO-1	U-DPO-2	U-DPO-3	U-DPO-4	U-DPO-5	U-DPO-6	U-DPO-7	U-DPO-8	U-DPO-9	U-DPO-10
DPO (mmol)	0.1	0.1	0.1	0.05	0.05	0.05	0.1	0.1	0.1	0.1
uranyl source	$UO_2(NO_3)_2\cdot 6H_2O$	$UO_2(NO_3)_2\cdot 6H_2O$	$UO_2(NO_3)_2\cdot 6H_2O$	$UO_2(CF_3SO_3)_2$	$UO_2(CF_3SO_3)_2$	$UO_2(CF_3SO_3)_2$	$UO_2(NO_3)_2\cdot 6H_2O$	$UO_2(NO_3)_2\cdot 6H_2O$	$UO_2(NO_3)_2\cdot 6H_2O$	$UO_2(NO_3)_2\cdot 6H_2O$
UO_2^{2+} (mmol)	0.05	0.05	0.05	0.025	0.025	0.025	0.05	0.05	0.05	0.05
solvent (mL)	H_2O	H_2O	H_2O	CH_3CN	CH_3CN	CH_3CN	H_2O	H_2O	H_2O	H_2O
	2	2	2	2	2	2	2	2	2	2
auxiliary ligand (mmol)	H_2MA 0.05						H_2TPA 0.05	H_2IPA 0.05	H_2SA 0.05	H_2SA 0.05
NaOH (1 M) (μL)		10	20					50	20	50
HNO_3 (4 M) (μL)										
pH	2.12	3.12	3.59				2.83	2.21	2.34	3.36
temp (°C)	R.T.	R.T.	150	120	120	120	150	150	R.T.	150

https://doi.org/10.1021/acsomega.3c00640
ACS Omega 2023, 8, 8894−8909

Table 2. Crystal Data and Refinement Details of All the Uranyl-DPO Compounds Ranging from U-DPO-1 to U-DPO-10

identification code	U-DPO-1	U-DPO-2	U-DPO-3	U-DPO-4	U-DPO-5
formula	$C_{10}H_{12}N_4O_{12}U$	$C_{10}H_8N_4O_{10}U$	$C_{10}H_{10}N_2O_6U$	$C_{22}H_{16}F_6N_4O_{12}S_2U$	$C_{22}H_{17}F_6N_4O_{13}S_2U$
f_w	618.27	582.23	492.23	944.54	961.55
T, K	294.97	292.76	298.28	297.00	273.15
crystal sys	triclinic	monoclinic	triclinic	monoclinic	tetragonal
space group	$P\bar{1}$	$C2/c$	$P\bar{1}$	$P2_1/n$	$I\bar{4}2d$
a, Å	5.9851(2)	16.2039(9)	7.4179(5)	10.6097(11)	23.2537(6)
b, Å	8.3549(3)	8.7697(4)	9.4446(7)	23.866(2)	23.2537(6)
c, Å	8.5969(3)	13.5603(7)	9.7682(6)	13.3086(14)	11.4512(4)
α, degree	82.8950(10)	90	75.670(3)	90	90
β, degree	76.1440(10)	116.234(2)	83.440(2)	103.625(5)	90
γ, degree	79.9520(10)	90	74.674(2)	90	90
V, Å^3	409.47(2)	1728.48(16)	638.61(8)	3275.0(6)	6192.1(4)
Dc (g·cm^{-3})	2.507	2.237	2.560	1.916	2.063
μ (mm^{-1})	9.986	9.447	12.733	5.179	5.483
F (000)	288	1072	448	1800	3672
R_{int}	0.0469	0.0365	0.0452	0.0641	0.1537
R_1, wR_2 [$I \geq 2\sigma(I)$]	0.0114, 0.0277	0.0263, 0.0539	0.0166, 0.0354	0.0431, 0.1010	0.0154, 0.0281
R_1, wR_2 (all data)	0.0124, 0.0279	0.0301, 0.0552	0.0195, 0.0366	0.0564, 0.1058	0.0188, 0.0283
identification code	U-DPO-6	U-DPO-7	U-DPO-8	U-DPO-9	U-DPO-10
formula	$C_{26}H_{20}F_3N_5O_{10}SU$	$C_{18}H_{12}N_2O_8U$	$C_{52}H_{32}N_4O_{29}U_4$	$C_{14}H_{14}N_2O_9U$	$C_{16}H_{15}N_2O_{13}U_2$
f_w	889.56	622.33	2128.93	592.30	919.36
T, K	282.31	296.06	297.64	295.54	296.45
crystal sys	monoclinic	monoclinic	monoclinic	monoclinic	monoclinic
space group	$P2_1/c$	$P2/c$	$C2/c$	$P2_1/c$	$P2/n$
a, Å	15.510(3)	7.1519(3)	35.205(5)	10.1492(19)	14.1065(16)
b, Å	18.580(4)	11.5518(3)	6.8919(12)	11.6946(19)	10.7833(13)
c, Å	14.734(3)	11.4531(3)	23.235(3)	14.417(2)	15.0099(18)
α, degree	90	90	90	90	90
β, degree	101.745(9)	90.3040(10)	96.982(5)	92.409(6)	111.510(4)
γ, degree	90	90	90	90	90
V, Å^3	4157.0(14)	946.21(5)	5595.6(15)	1709.7(5)	2124.2(4)
Dc (g·cm^{-3})	1.421	2.184	2.527	2.301	2.875
μ (mm^{-1})	4.015	8.627	11.641	9.546	15.301
F (000)	1704	580	3888	1104	1652
R_{int}	0.0574	0.0406	0.0732	0.0977	0.1096
R_1, wR_2 [$I \geq 2\sigma(I)$]	0.0289, 0.0753	0.0329, 0.0836	0.0657, 0.1695	0.0589, 0.1444	0.0301, 0.0815
R_1, wR_2 (all data)	0.0348, 0.0781	0.0355, 0.0858	0.1265, 0.2087	0.0861, 0.1637	0.1047, 0.0979

function (ELF)[69,70] analysis were performed by Multiwfn software 3.6.[71]

RESULTS AND DISCUSSION

Structure Description of All Uranyl-DPO Compounds. U-DPO-1 ($(UO_2)(NO_3)_2(H_2O)_2\cdot(DPO)$) was prepared through evaporation from water. Crystallographic analysis reveals that it is a cocrystal compound of uranyl nitrate hydrate and DPO (Figures 1 and S2a) that crystallizes in the $P\bar{1}$ space group (Table 2). It is noted that, though H_2MA is added together with DPO, it is not present in the final crystallization product. In U-DPO-1, the only uranyl center is 8-fold coordinated, resembling the coordination geometric structure of uranyl in uranyl nitrate hydrate: two axial oxygen atoms and six equatorial oxygen atoms from two water molecules (U−$O(H_2O)$, 2.406(2) Å) and two bidentate coordinated nitrate ions (U−$O(NO_3^-)$, 2.500(2) and 2.533 (2) Å) (Figure 1a). Interestingly, DPO molecules are not involved in the uranyl coordination sphere but connect with the uranyl coordination units by several hydrogen bonds (Figure 1b). With the bridging of DPO, a two-dimensional supramolecular network is formed by alternate arrays of uranyl units and DPO units (Figure 1c,d). Further, intensive $\pi-\pi$ interactions between bipyridine rings of DPO ligands with a spacing of ∼3.327 Å between adjacent planes (Figure S3) result in a close packed 3D lattice in U-DPO-1 (Figure 1e).

Crystallographic analysis of U-DPO-2 ($(UO_2)(NO_3)_2(DPO)$) shows that it crystallizes the $C2/c$ space group with a 1D chain structure (Figure 2), which is previously reported by Muthiah et al.[60] In U-DPO-2, the uranyl cation is also eight-coordinated, which is similar to that of U-DPO-1. Besides two axial oxygen atoms with equivalent [U≡O_{ax}] bonds of 1.765(3) Å, the uranium center is coordinated by two equivalent nitrate ions and two equivalent DPO ligands on the equatorial plane, where both the nitrate ions take a chelated coordination mode (U−$O(NO_3^-)$, 2.540(3) and 2.540(4) Å), while the DPO ligand is monocoordinated to uranyl by one of its end oxygen atoms (U−O(DPO), 2.360(3) Å) (Figures 3a and S2b). Two nitrate ions are symmetrically distributed on the equatorial plane of uranyl center, and the bidentate DPO ligand further bridges two uranyl cation centers through both ends forming a 1D extended chain (Figure 2b). Since there is an inclined angle of 66.09° between the equatorial plane of the uranium center and the adjacent pyridine ring, the 1D extended

https://doi.org/10.1021/acsomega.3c00640
ACS Omega 2023, 8, 8894−8909

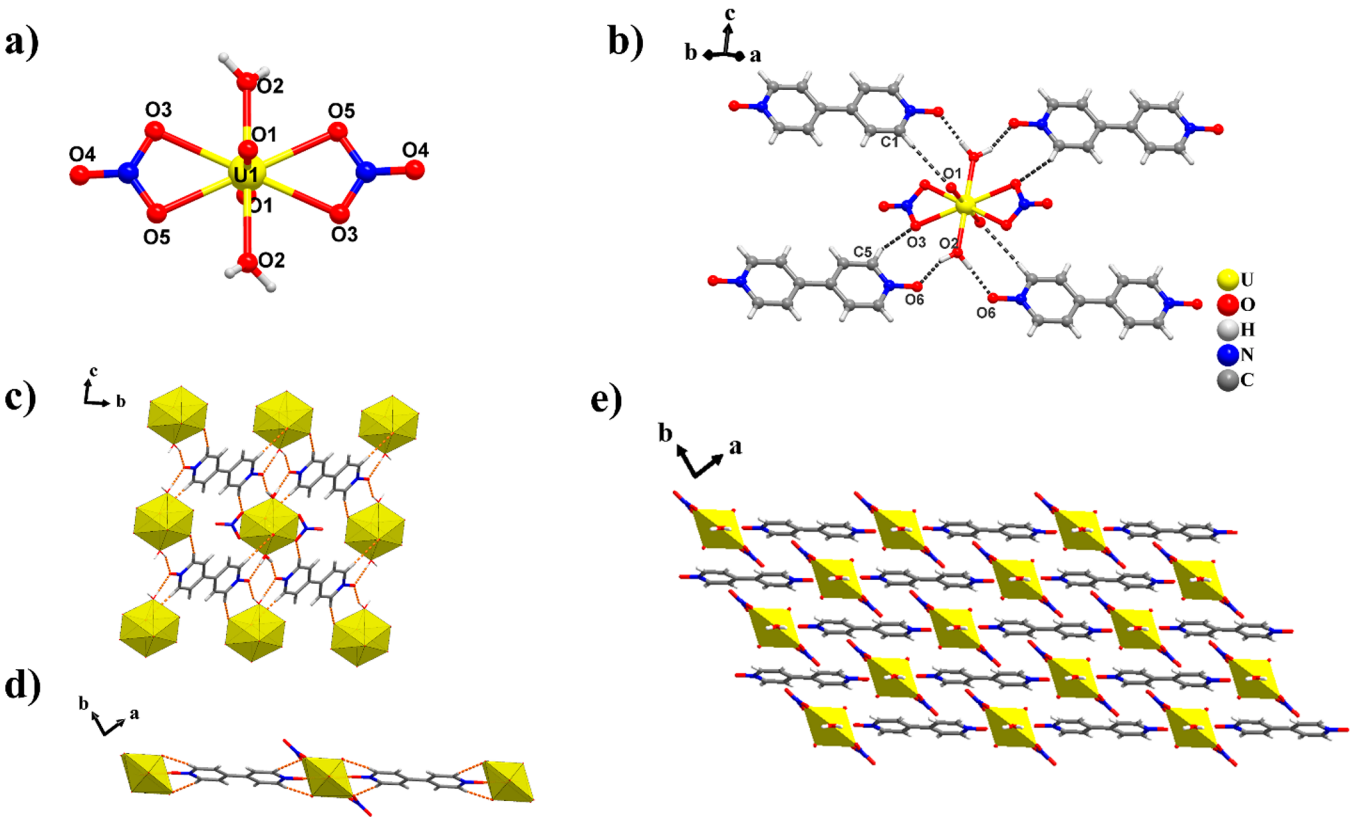

Figure 1. Crystal structure and lattice stacking of U-DPO-1: (a) coordination sphere of uranyl center in U-DPO-1; (b) hydrogen bonds between the uranyl nitrate unit and free DPO molecules in U-DPO-1 (distance between hydrogen atom to oxygen donor: O(2)−H(2A)···O(6), 1.841(2) Å; O(2)−H(2B)···O6, 1.811(2) Å; C(1)−H(1)···O(1), 2.799(2) Å; C(5)−H(5)···O(3), 2.604(2) Å); (c, d) lattice stacking diagram along the plane perpendicular to *a*-axis (c) and *c*-axis (d) showing that two-dimensional supramolecular networks formed by each of the uranyl units and DPO units stack alternately; (e) the molecular stacking in a 3D lattice of U-DPO-1.

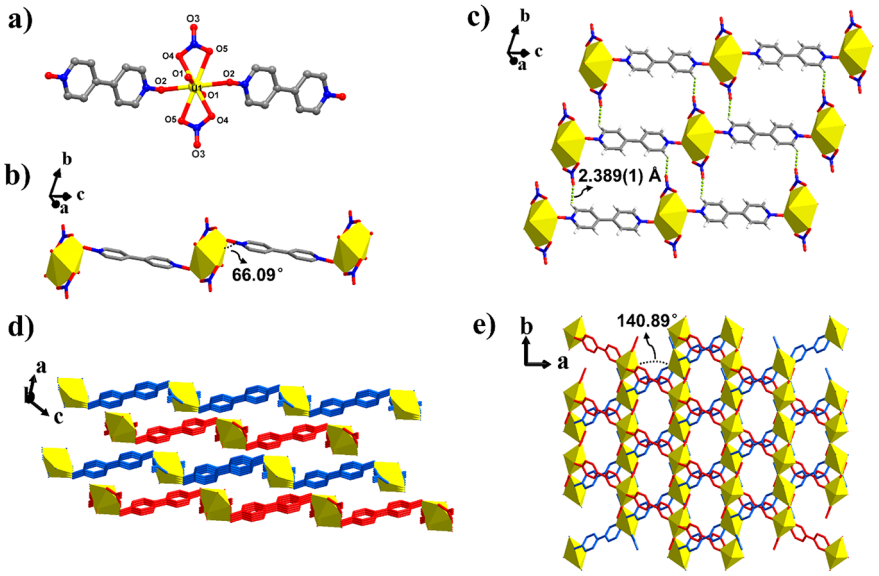

Figure 2. Crystal structure of U-DPO-2: (a) coordination sphere of uranyl cation in U-DPO-2; (b) 1D extended zigzag chain of U-DPO-2 with a torsion angle of 66.09°; (c) hydrogen bonds between adjacent 1D chains in U-DPO-2 (distance between hydrogen atom to oxygen donor: C(1)−H(1)···O(3), 2.389(1) Å); (d) lattice stacking of 2D hydrogen bonded networks in U-DPO-2; (e) different extension directions of the 1D chain units in adjacent hydrogen bond networks with an angle of 140.89°.

chain takes a zigzag shape. Furthermore, the 1D uranyl-DPO chains are arranged side by side in the same layer with intensive interchain hydrogen bonds between C−H motifs of the pyridine rings and oxygen atoms of nitrate ions (C(1)−H(1)···O(3) hydrogen bond with a H(1)···O(3) distance of 2.389 Å) (Figure 2c). The resultant 2D hydrogen bonded networks are stacked closely in the 3D lattice (Figure 2d), though the extension directions of the 1D chain units in adjacent hydrogen bond

https://doi.org/10.1021/acsomega.3c00640
ACS Omega 2023, 8, 8894−8909

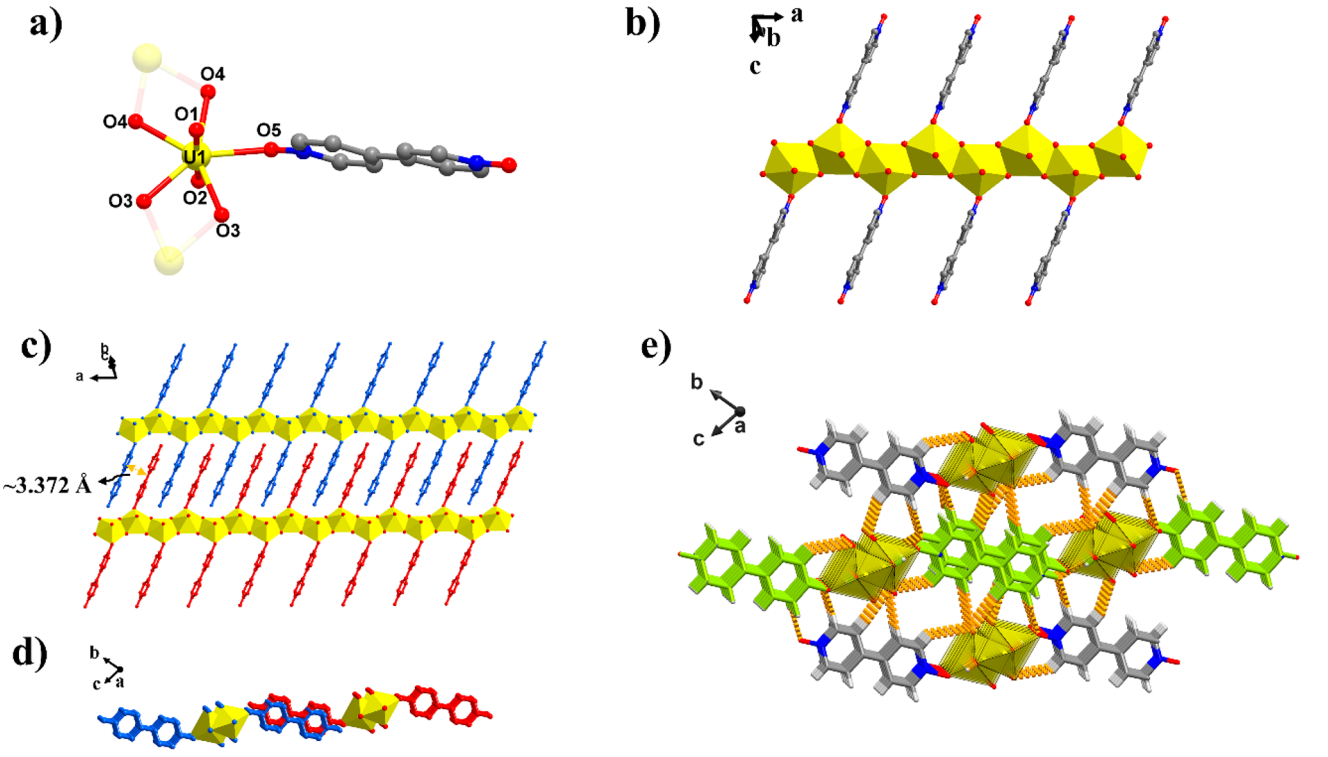

Figure 3. Crystal structure of U-DPO-3: (a) coordination sphere of the uranyl center; (b) 1D extension of polymeric uranyl chain in U-DPO-3; (c) the 2D extension of uranyl coordination chains by $\pi-\pi$ stacking with a spacing of ~3.372 Å between adjacent planes; (d) $\pi-\pi$ stacking-based 2D supramolecular network viewed from the *a*-axis; (e) 3D-space lattice stacking of an array of 2D networks through intensive hydrogen bonds (distance between hydrogen atom to oxygen donor: C(1)−H(1)···O(1), 2.587(3) Å; C(2)−H(2)···O(1), 2.466(3) Å; C(5)−H(5)···O(1), 2.799(3) Å; C(6)−H(6)···O(5), 2.385(3) Å; C(10)−H(10)···O(6), 2.443(3) Å; C(9)−H(9)···O(2), 2.506(3) Å).

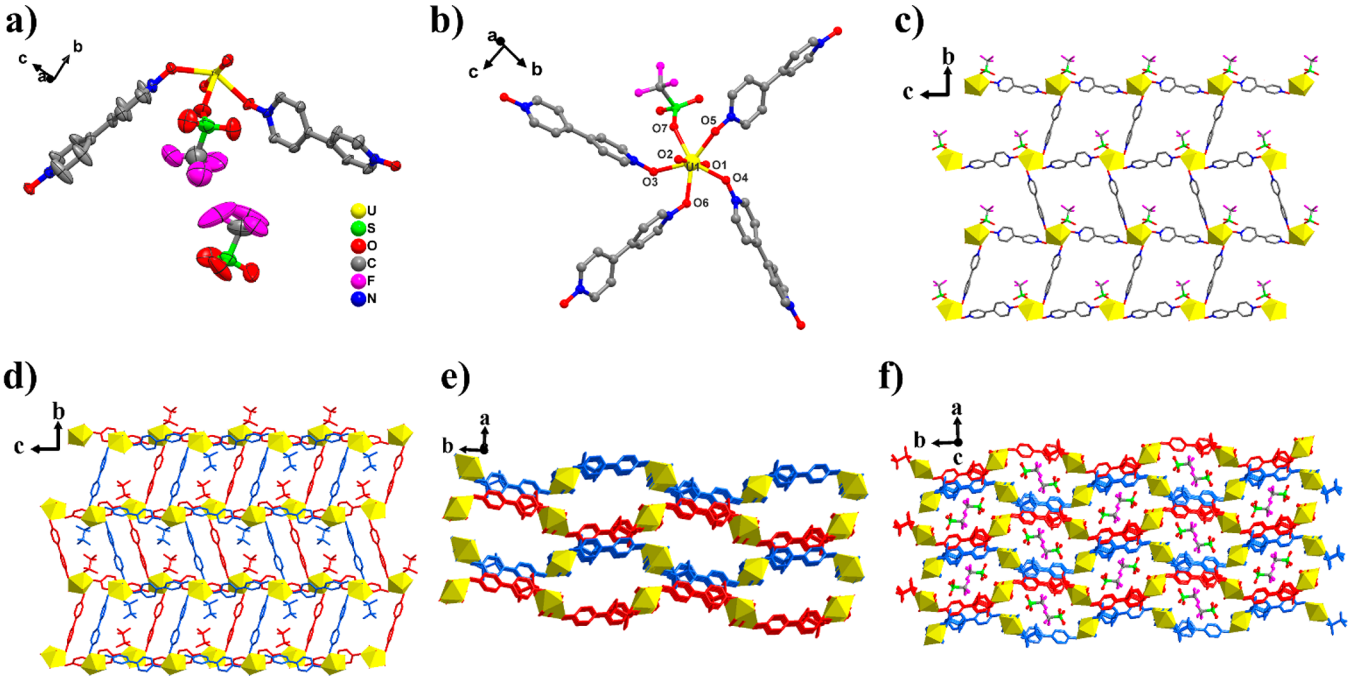

Figure 4. Crystal structure of U-DPO-4: (a) the asymmetric unit of U-DPO-4 with thermal ellipsoids shown at 50% probability; (b) coordination environment of the uranyl center in U-DPO-4; (c) 2D coordination network structure of U-DPO-4; (d) the lattice stacking of the 2D networks in U-DPO-4 viewed from the *a*-axis; (e) the lattice stacking of the 2D networks viewed from the *c*-axis to give a 3D supramolecular framework; (f) free $CF_3SO_3^-$ counterions filling in the cavities of the 3D framework in U-DPO-4.

networks are not in parallel but have an angle of 140.89° (Figure 2e).

Crystallizing in space group of $P\bar{1}$, U-DPO-3 ($(UO_2)(DPO)$-$(\mu_2\text{-}OH)_2$) has an infinite polymeric chain structure that is bridged all by μ_2-hydroxyl oxygen atoms (Figure 3). The [O_{ax}≡

https://doi.org/10.1021/acsomega.3c00640
ACS Omega 2023, 8, 8894−8909

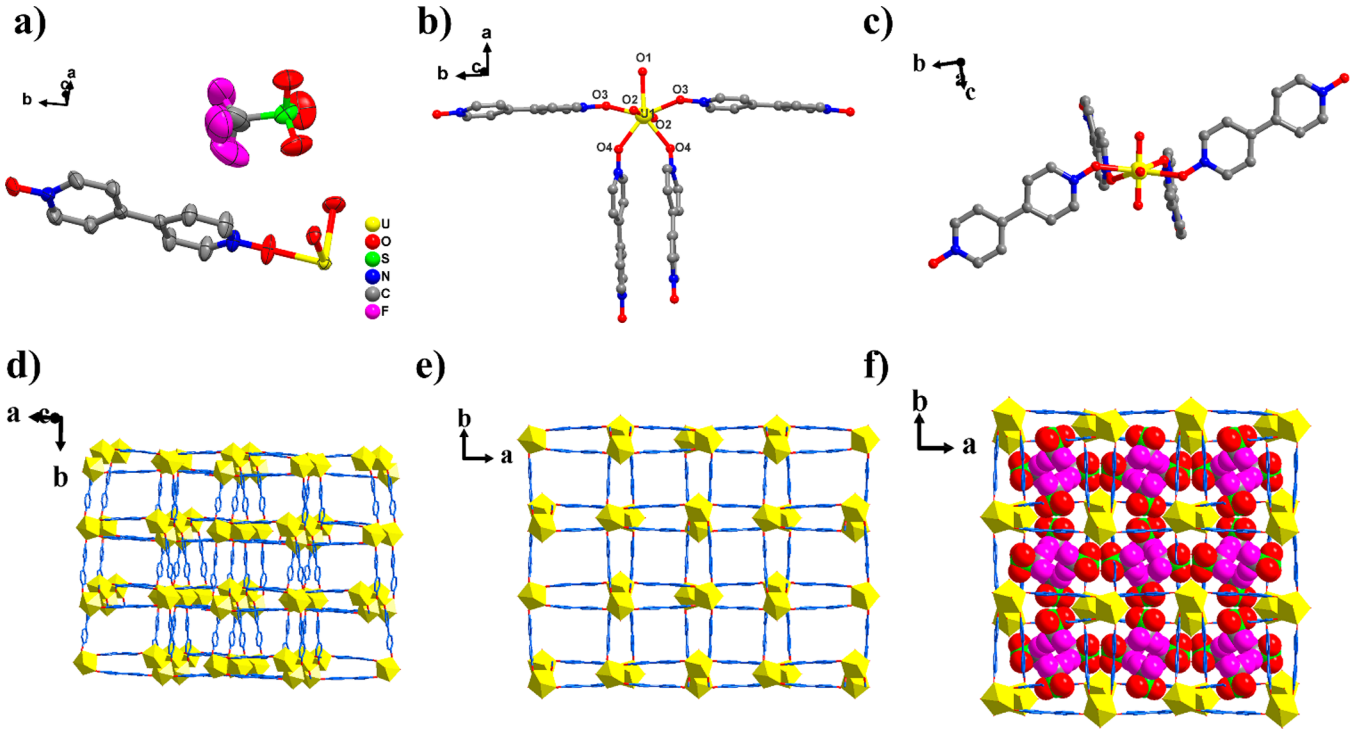

Figure 5. Crystal structure of U-DPO-5: (a) the asymmetric unit of U-DPO-5 with thermal ellipsoids shown at 50% probability; (b) uranyl coordination environment of the mononuclear uranyl center of U-DPO-5; (c) the twisted alignment of four DPO ligands around the uranium center in U-DPO-5; (d) the 3D supramolecular framework in U-DPO-5; (e) the channels of the 3D framework in U-DPO-5; (f) $CF_3SO_3^-$ counterions filling in channels of the 3D framework in U-DPO-5.

$U{\equiv}O_{ax}$] angle of the uranyl cation is 177.61(14)° with an equivalent [$U{\equiv}O_{ax}$] distance of 1.780(4) Å. Each 7-fold coordinated uranyl cation in the polymeric uranyl chain has five oxygen atoms coordinated in its equatorial plane: four oxygen atoms from μ_2-hydroxyl groups (U−O(μ_2-OH), 2.348(3), 2.351(3), 2.340(3), and 2.334(3) Å) and another one from a monocoordinated DPO ligand with a slightly longer U−O distance (U−O(DPO), 2.441(3) Å) (Figure 3a). It is notable that, while a ditopic DPO ligand generally serves as a biconnected linker through two-end uranyl coordination,[57−60,72] such a monodentate coordinated DPO is rarely reported, only being found in DPO ligands enclosed by cucurbituril macrocycles.[44] All these monodentate DPO ligands are arranged alternately on both sides of the "spine" of the μ_2-hydroxyl bridged uranyl chain, thus forming a "fishbone" shape (Figure 3b). There is enough room between every two adjacent ligands on the same side of the uranyl chain, leaving space for a neighboring U-DPO-3 chain to insert via a $\pi-\pi$ stacking interaction with a spacing of ∼3.372 Å between adjacent planes. Hirshfeld surface analysis of DPO motifs in U-DPO-3 using CrystalExplorer program[73] was conducted and compared with that in U-DPO-1 (Figure S4). The fingerprint plot of a couple of DPO molecules in U-DPO-3 shows up as a typical dark region in the vicinity of (d_i, d_e) ∼ 1.7−1.8 Å,[74] which is consistent with the interplanar spacing of DPO. In contrast, given that the stacking in U-DPO-1 involves only partial overlap of the DPO units, unlike complete overlap in U-DPO-3, it is reasonable to see that the dark region in the fingerprint plot for U-DPO-1 is not that obvious. The 1D coordination chains can be stacked through the above-mentioned $\pi-\pi$ interactions, forming an extended 2D network structure (Figure 3c). Again, since the extension direction of the DPO side group deviates from the plane of the polymeric uranyl chain, the two-dimensional chain formed by the $\pi-\pi$ interaction is not an ideally planar structure but has a certain fluctuation (Figure 3d), which stacks with each other to realize the 3D-space lattice packing of U-DPO-3 through intensive hydrogen bonds (Figure 3e).

When a different uranyl source $UO_2(CF_3SO_3)_2$, instead of uranyl nitrate hydrate, is used to react with DPO, new uranyl compounds with $CF_3SO_3^-$ ions involved as coordinated anions (U-DPO-4) and/or counterions (U-DPO-4, U-DPO-5, and U-DPO-6) could be obtained. U-DPO-4 ($[(UO_2)(CF_3SO_3)(DPO)_2](CF_3SO_3)$) crystallizes in the $P2_1/c$ space group with a 2D network structure. The mononuclear uranyl center is seven-coordinated (Figure 4a,b). In the equatorial plane, there are five oxygen atoms coordinated with the uranyl center: four from four different DPO ligands and another one from a $CF_3SO_3^-$ anion. The lengths of U−O bonds are in the range of 2.334(5)−2.418(6) Å (Table S1). Four DPO ligands around the uranyl center are all aligned as twisted quadrilaterals and further extend out as ditopic ligands to form a planar 2D network within the plane perpendicular to the c-axis (Figure 4c). The uranyl-DPO 2D network with a coordinated $CF_3SO_3^-$ anion is similar to a previously reported uranyl-DPO compound with Keggin-type polyoxometalate as coordinated anion and cavity-filling agent,[58] which might be related to the fact that this network structure has enough room to accommodate anions with different sizes. Adjacent layers of 2D networks pack with each other in an antiparallel manner (Figure 4d) via intensive weak interactions such as hydrogen bonds in the lattice to form a final 3D supramolecular framework (Figure 4e). It is interesting to find that, unlike the case of compounds U-DPO-1, U-DPO-2, and U-DPO-3 using uranyl nitrate in an aqueous environment, U-DPO-4 that was prepared from $UO_2(CF_3SO_3)_2$ in nonaqueous solvent turns out to be a cationic framework, though the coordinated $CF_3SO_3^-$ partially offset the positive charge of the

https://doi.org/10.1021/acsomega.3c00640
ACS Omega 2023, 8, 8894−8909

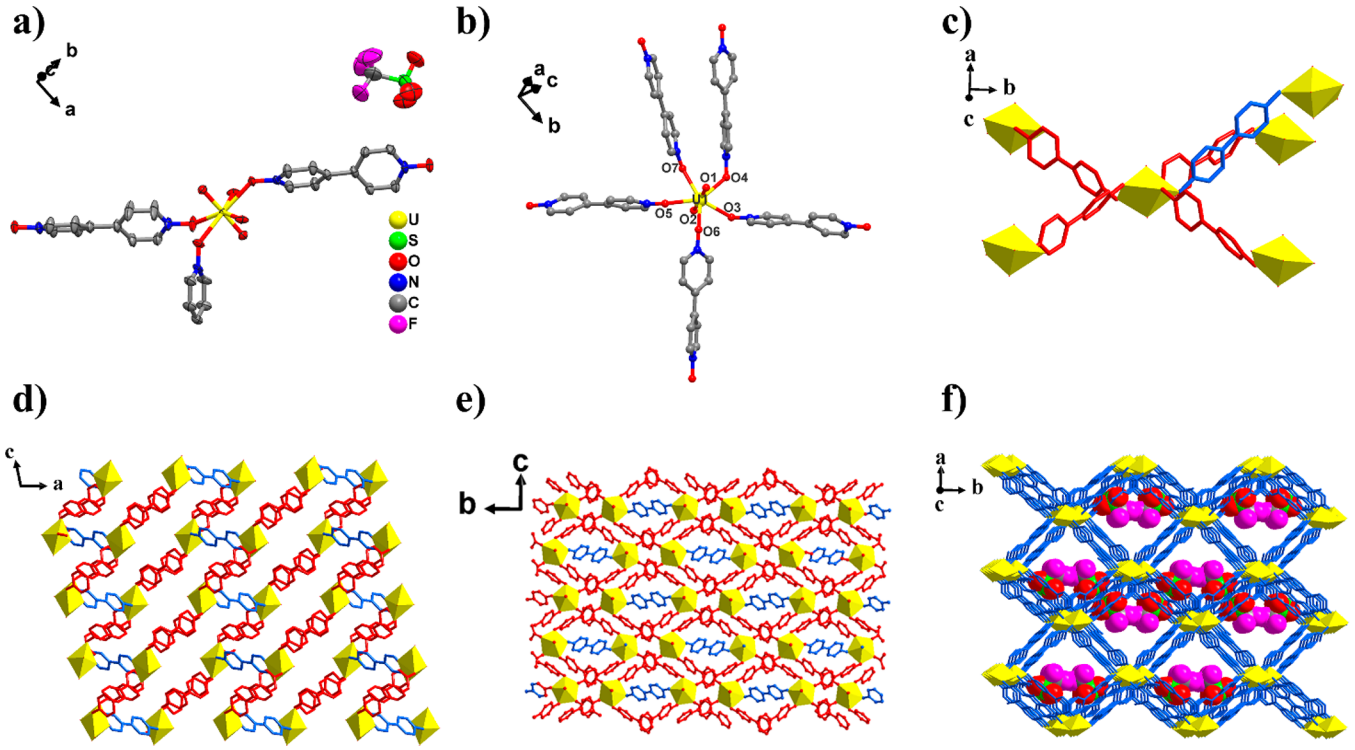

Figure 6. Crystal structure of U-DPO-6: (a) the asymmetric unit of U-DPO-6; (b) coordination environment of the uranyl center in U-DPO-6; (c) a comparison of five DPO ligands in U-DPO-6 pointing to different directions; (d) the 3D structure linked by two kinds of DPO ligands; (e) the 3D structure linked by two kinds of DPO ligands viewed along the *c*-axis; (f) free $CF_3SO_3^-$ ions filling in the channels of the 3D framework of U-DPO-6.

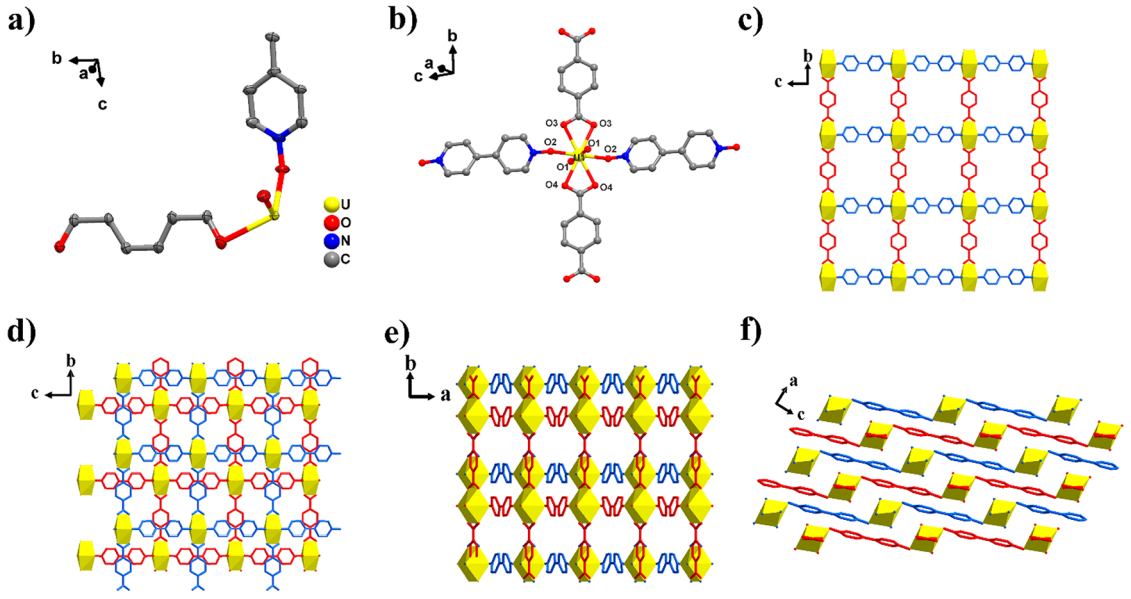

Figure 7. Crystal structure of U-DPO-7: (a) the asymmetric unit of U-DPO-7; (b) the coordination sphere of 8-fold coordinated uranyl cation center in U-DPO-7; (c) the 2D coordination network based on TPA^{2-} and DPO ligand in U-DPO-7; (d) "ABAB" stacking between the 2D layered networks in U-DPO-7; (e) the stacking pattern of the 2D layered networks viewed from the *c*-axis; (f) packing of coordination layers in the 3D lattice of U-DPO-7.

framework. Since the 2D network is extended in a serpentine style, there are channels with proper sizes in the 3D cationic framework for accommodating free $CF_3SO_3^-$ counterions for charge balance (Figure 4f).

Crystallographic analysis of U-DPO-5 ($[UO_2(H_2O)(DPO)_2](CF_3SO_3)_2$) reveals that it crystallizes in the $I\bar{4}2d$ space group with a 3D coordination framework structure. In the asymmetric unit of U-DPO-5 (Figure 5a), the uranyl center is seven-coordinated with four DPO ligands (U−O(DPO), 2.330(4) and 2.349(3) Å)) and one water molecule (U−$O(H_2O)$, 2.431(5) Å) coordinated in the equatorial plane (Figure 5b). The unexpected water molecule coordinating with the uranyl cation is presumed to originate from residual water in CH_3CN solvent. Four DPO ligands around the uranium center

https://doi.org/10.1021/acsomega.3c00640
ACS Omega 2023, 8, 8894−8909

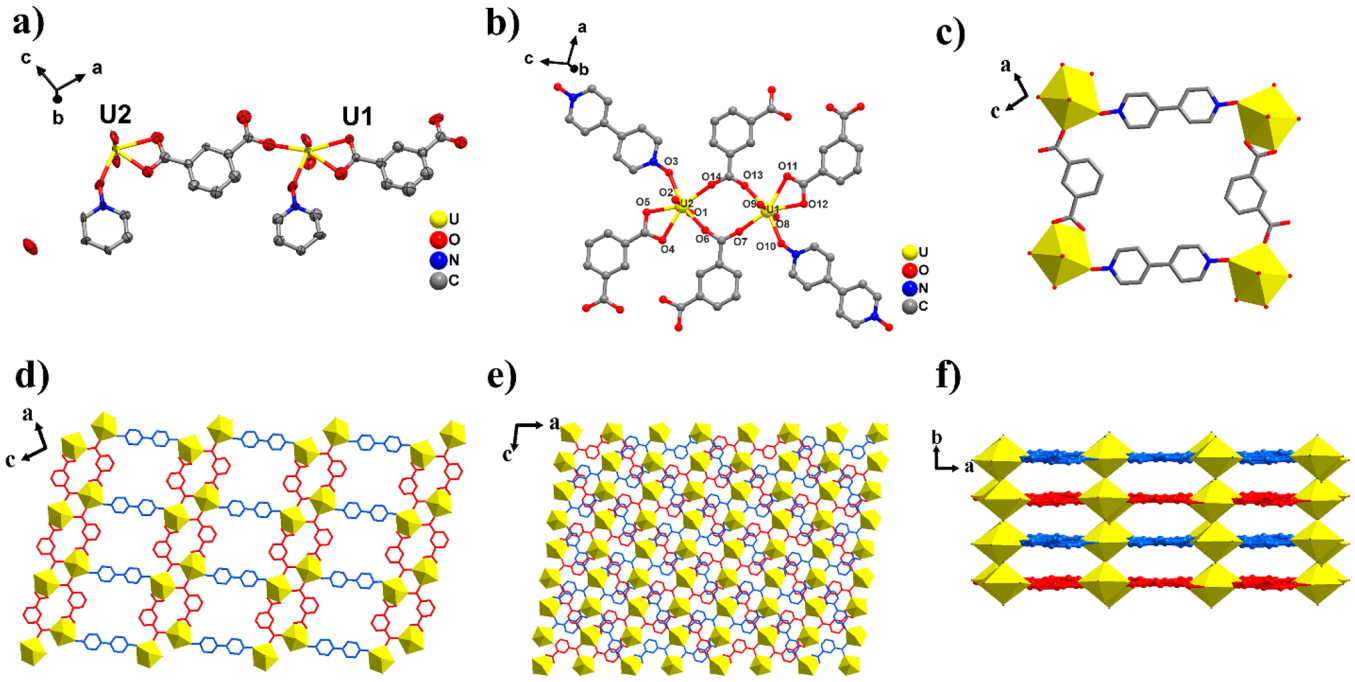

Figure 8. Crystal structure of U-DPO-8: (a) the asymmetric unit of U-DPO-8; (b) coordination environment of the uranyl center in U-DPO-8; (c) the rectangular ring unit based on DPO and IPA^{2-} ligands; (d) 2D network structure of U-DPO-8; (e) stacking of adjacent coordination networks with slight sliding; (f) stacking of coordination networks in the 3D lattice of U-DPO-8 viewed along the *b*-axis.

in U-DPO-5 align in a twisted geometry and point toward different directions in 3D space (Figure 5c) to form a 4-connected unit, which finally results in a 3D cationic coordination framework structure (Figure 5d). Along the *c*-axis, there are two kinds of channels in the framework of U-DPO-5 (Figure 5e), among which the smaller one is formed by two DPO ligands with a rectangular shape and the larger one is formed by four DPO ligands with an approximately square shape. Further, $CF_3SO_3^-$ ions that originate from the $UO_2(CF_3SO_3)_2$ source all fill in the channels of 3D framework as counterions (Figure 5f). This result shows that the combination of aprotic DPO ligand with uranyl ion successfully produces the U-DPO-5 compound with a cationic framework structure that can be a potential candidate as anion exchange material, which is distinct from those neutral or anionic uranyl frameworks built from carboxylate or phosphonate ligands.[39,41]

U-DPO-6 ($[(UO_2)(DPO)_{2.5}](CF_3SO_3)_2$) crystallizes in the $P2_1/c$ space group with a 3D framework structure. As shown in Figure 6a,b, the uranyl cation center has similar 7-fold coordinated geometry with that observed in U-DPO-4 and U-DPO-5. A slight difference is that all the five oxygen donors on the equatorial plane are provided by five different DPO ligands with U−O lengths in the range of 2.369(3)−2.423(3) Å (Table S2). According to the spatial orientation of DPO linkers, these five DPO ligands around the uranyl center can be classified into two categories (Figure 6c): first, four DPO ligands (highlighted in red color) bridge uranyl cation centers (O-donors: O3 and O4, O5 and O6) in the same layer, forming a 2D network; second, the fifth DPO ligand (highlighted in blue color) pointing out the layer connects adjacent layers of networks (O-donor: O7) to form a final 3D framework (Figure 6d,e). Specifically, viewed along the *b*-axis, four DPO ligands first bridge the uranyl center forming a 2D layer, and the fifth DPO ligand coordinates with two uranyl centers from two layers, leaving a 3D framework with a lot of channels along the *b*-axis (Figure 6d). Viewed along the *a*-axis, the quadrilateral cavities formed from the four DPO ligands are blocked by the fifth DPO ligands (Figure 6e). Along the *c*-axis, a large number of channels can be seen, where there are a lot of free $CF_3SO_3^-$ ions as counterions of the cationic 3D framework (Figure 6f).

Uranyl compounds containing both DPO and organic dicarboxylic acid as ligands are also synthesized. U-DPO-7 ($(UO_2)(TPA)(DPO)$) was prepared from a DPO and H_2TPA mixed-ligand system. Single-crystal structure analysis reveals that it crystallizes in the $P2/c$ space group with a monomeric uranyl center, which is totally different from the tetrameric uranyl-based product from a similar mixed-ligand reaction system.[59] As shown in Figure 7a,b, the uranyl center is 8-fold coordinated, including two axial oxygen atoms and six equatorial oxygen atoms from two DPO ligands and two TPA^{2-} ligands in η^2-chelating mode. In the equatorial plane, U−O bond lengths are 2.390(5) Å (U(1)−O(2)) for the DPO ligand and 2.520 (5) Å (U(1)−O(3)) and 2.522 (5) Å (U(1)−O(4)) for η^2-TPA^{2-}. The TPA^{2-} and DPO ligands coordinate with the uranyl center in a symmetrical pattern, forming a rectangular 2D network (Figure 7c). In the plane perpendicular to the *a*-axis, the layered networks are divided into two groups and align orderly in an "ABAB" pattern. Although there are large cavities in each ordered rectangular network, the sliding of the neighboring layers partly block the voids of the cavities and reduce the size of the channels (Figure 7d,e). Furthermore, these 2D networks show a stacking mode similar to U-DPO-2 through hydrogen bonds between adjacent 2D networks from axial oxygen atoms and C−H motifs of DPO (Figure S5), resulting in a final 3D supramolecular framework (Figure 7f).

Starting from DPO and H_2IPA, another uranyl-DPO compound with 2D network structure, U-DPO-8 ($(UO_2)_2(DPO)(IPA)_2{\cdot}0.5H_2O$), is obtained. It crystallizes in the $C2/c$ space group with two crystallographically non-equivalent uranyl cations (U1 and U2, Figure 8a). Different

https://doi.org/10.1021/acsomega.3c00640
ACS Omega 2023, 8, 8894−8909

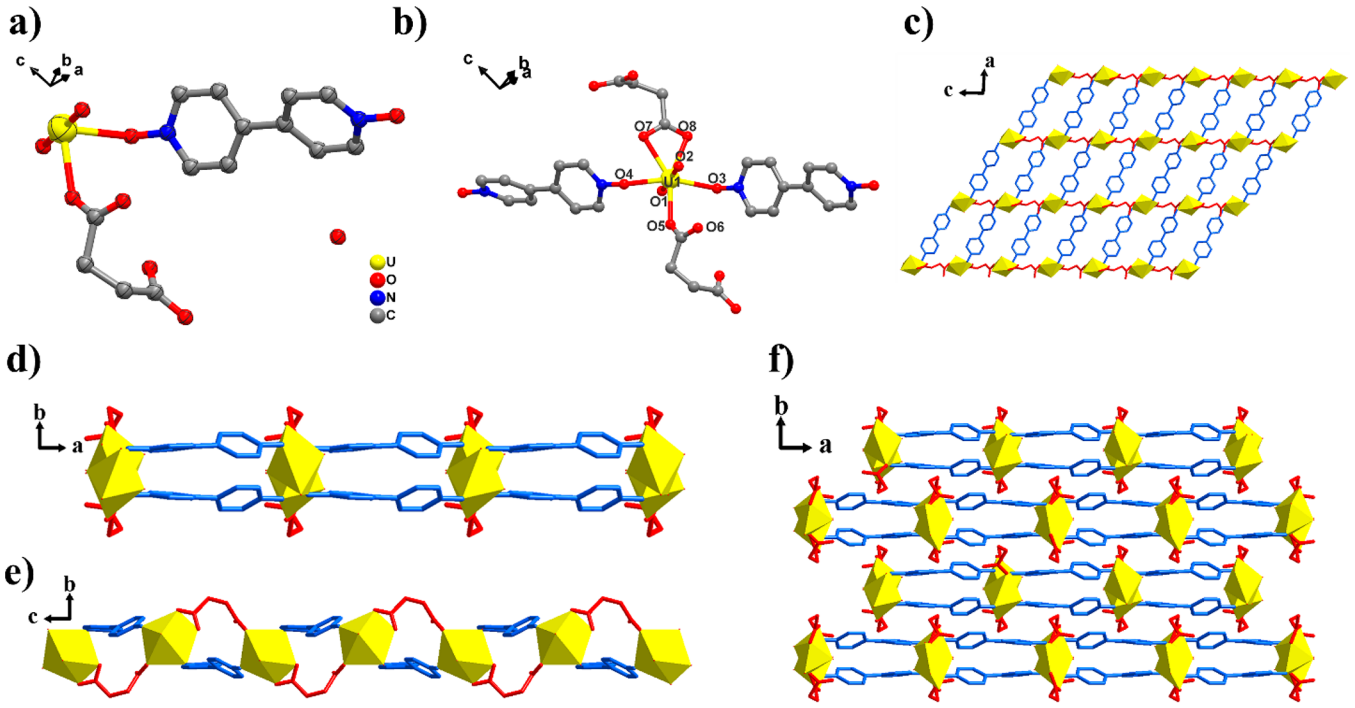

Figure 9. Crystal structure of U-DPO-9: (a) the asymmetric unit of U-DPO-9; (b) the coordination environment of the uranyl cation center in U-DPO-9; (c) the 2D network extending through the connection of SA^{2-} and DPO ligands with uranyl in U-DPO-9; (d, e) the 2D coordination networks in U-DPO-9 viewed from the *c*-axis (d) and *a*-axis (e), respectively; (f) the lattice packing of 2D networks in U-DPO-9.

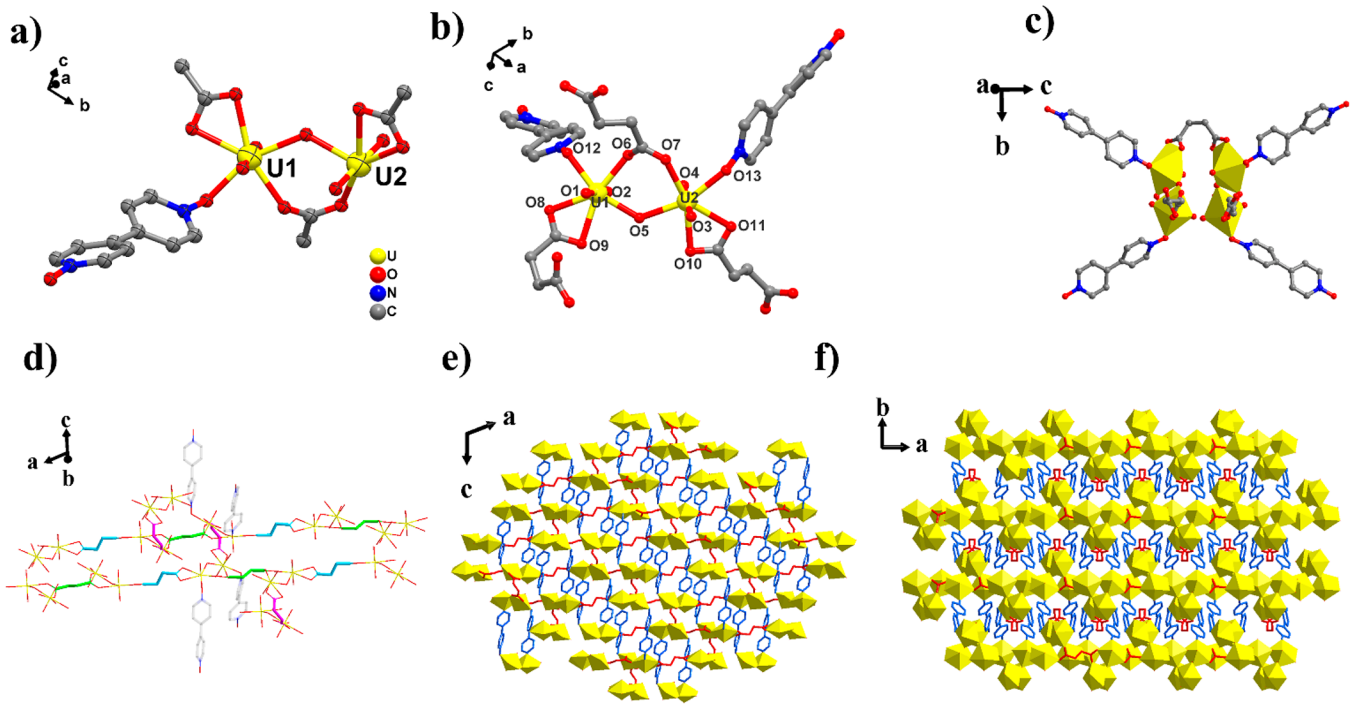

Figure 10. Crystal structure of U-DPO-10: (a) the asymmetric unit of U-DPO-10; (b) the coordination environment of two uranyl centers of binuclear uranyl node in U-DPO-10; (c) arc-like SA^{2-} ligands for linking two binuclear uranyl centers in U-DPO-10; (d) three kinds of SA^{2-} ligands contributing to build up the framework of U-DPO-10 (blue color, bidentate chelating coordination modes in a normal staggered conformation with the whole alkyl chains being stretched; green color, μ_2-(η^1,η^1) bridging bidentate pattern in a stretched shape; pink color, bidentate coordination modes at both ends is of arc-like geometry; (e) the spatial packing of U-DPO-10 in 3D lattice viewed from the *b*-axis (DPO, blue; succinate, red; uranyl polyhedron, yellow); (f) the spatial packing of U-DPO-10 in a 3D lattice viewed from the *c*-axis.

from the monomeric uranyl node in U-DPO-7, all the uranyl nodes occur in pairs through the bridging bidentate coordination of a pair of carboxyl groups from two IPA^{2-} ligands (Figure 8b). Each uranyl in the dimeric motif coordinates with seven oxygen atoms and has a similar coordination environment. Besides the two axial oxygen atoms, there is one oxygen atom

https://doi.org/10.1021/acsomega.3c00640
ACS Omega 2023, 8, 8894−8909

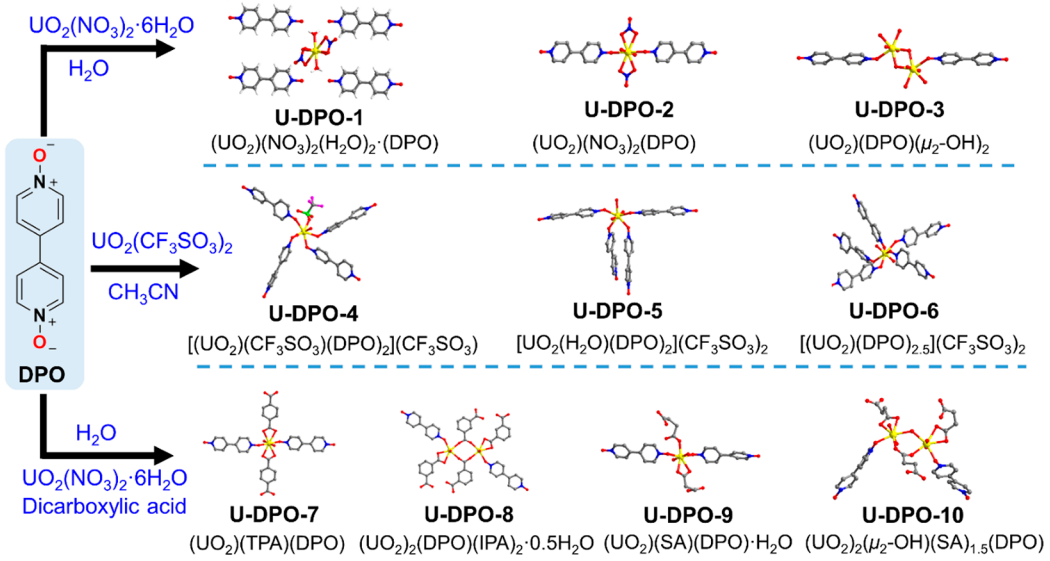

Figure 11. Preparation of ten uranyl DPO compounds though coordination assembly between uranyl and DPO based on different synthesis procedures. U-DPO-1, U-DPO-2, and U-DPO-3: DPO with uranyl nitrate in water; U-DPO-4, U-DPO-5, and U-DPO-6: DPO with uranyl triflate in acetonitrile; U-DPO-7, U-DPO-8, U-DPO-9, and U-DPO-10: DPO and dicarboxylic acid (H_2TPA for U-DPO-7, H_2IPA for U-DPO-8, H_2SA for U-DPO-9 and U-DPO-10) with uranyl nitrate in water.

from a DPO ligand (U−O(DPO), 2.37(2) and 2.370(19) Å) and four oxygen atoms from three IPA^{2-} ligands: two in bidentate-bridging mode (U−O(μ_2-IPA^{2-}), 2.27(2), 2.279(19), 2.31(2), and 2.32(2) Å) and one in bidentate mode (U−O(η^2-IPA^{2-}), 2.53(2), 2.345(19), 2.496(15), and 2.394(19) Å). The binuclear uranyl-IPA nodes extend to form ladder-like chains, which are further connected by DPO ligands to form a 2D network structure with rectangular ring units (Figure 8c,d). It is noted that, in spite of the presence of dimeric uranyl nodes in U-DPO-7, the total structure and local structural unit (Figure S6) of U-DPO-8 is still similar to U-DPO-7. Furthermore, the coordination layers accumulate together along the *b*-axis with a slight sliding (Figure 8e) and finally afford a dense packing structure for U-DPO-8 (Figure 8f).

Crystallographic analysis of U-DPO-9 ($(UO_2)(SA)(DPO)\cdot H_2O$) reveals that it crystallizes in the $P2_1/c$ space group with a 2D network structure. Apart from two axial oxygen atoms, the 7-fold coordinated uranyl cation center coordinates with two DPO ligands and two carboxyl groups from two different succinate ligands on its equatorial plane. Two carboxyl groups at two ends of each succinate ligand are bidentate chelated and monodentate-coordinated, respectively (Figure 9a,b). All the U−O bond lengths on the equatorial are in the range from 2.297(13) to 2.463(11) Å, where U−O(DPO) bond lengths are 2.350(9) and 2.369(10) Å, while U−O(SA^{2-}) bond lengths are 2.297(13) Å for the monodentate carboxyl group and 2.446(13) and 2.463(11) Å for the bidentate one. As is shown in Figure 9c, the SA^{2-} ligands are arranged in line along the *c*-axis to give 1D chains, which are further connected by ditopic DPO linker to form a 2D network. Although the resultant 2D network is similar to that in U-DPO-7, the flexible SA^{2-} linkers have more distorting *cis*-conformation compared to TPA^{2-} in U-DPO-7 and lead to obvious wrinkles of the 2D networks (Figure 9d,e). Figure 9f shows the lattice packing of these 2D coordination networks in U-DPO-9.

U-DPO-10 ($((UO_2)_2(\mu_2\text{-}OH)(SA)_{1.5}(DPO))$) crystallizes in the $P2/n$ space group with a 3D framework structure. Both uranyl centers from the binuclear uranyl node are 7-fold coordinated. The [U≡O_{ax}] bond lengths are in the range of 1.766(6) and 1.776(6) Å with the angles of [O_{ax}≡U≡O_{ax}] being 178.7(3)° (U1) and 178.3(3)° (U2). Two uranyl cations in the binuclear uranyl center are connected with a μ_2-hydroxyl oxygen atom (U−O(hydroxyl), 2.348(6) and 2.334(6) Å) and a μ_2-(η^1, η^1) bridging carboxyl group from a SA^{2-} ligand (U−O(μ_2-SA^{2-}), 2.301(7) and 2.401(5) Å) (Figure 10a). Meanwhile, with a similar coordination environment, each uranyl center in binuclear motif further coordinates with one DPO ligand (U−O(DPO), 2.359(5) and 2.363(7) Å) and a second bidentate chelating SA^{2-} ligand, respectively (U(1)-O(η^2-SA^{2-}), 2.421(7) and 2.472(7) Å; U(2)-O(η^2-SA^{2-}), 2.489(6) and 2.479(5) Å) (Figure 10b). Similar to the *cis*-conformation of flexible SA^{2-} ligand observed in U-DPO-9, SA^{2-} ligands that take a folding conformation to bridge two adjacent binuclear uranyl centers are also present in U-DPO-10 (Figure 10c). Actually, there are a total of three different kinds of SA^{2-} ligands in U-DPO-10: the first one that bridges two uranyl cations via bidentate chelating coordination modes at both ends of SA^{2-} ligands has a normal staggered conformation with the whole alkyl chain being stretched (Figure 10d, in blue color); the second one that connects two binuclear uranyl centers via a μ_2-(η^1, η^1) bridging bidentate pattern for each carboxyl group at both ends also takes a stretched shape (Figure 10d, in green color); the third one, as mentioned above, bridges two binuclear uranyl centers via bidentate coordination modes at both ends is of arc-like geometry (Figure 10d, in pink color). The two kinds of stretched SA^{2-} ligands coordinate with uranyl nodes to form an array of 1D chains, which are further connected by the third arc-like SA^{2-} ligands (Figure 10e). Furthermore, based on the SA^{2-} ligand-connected networks that are arranged along the *ac* plane, DPO ligands cross-link these layers to form the final 3D framework (see Figure 10f; the SA^{2-} auxiliary ligands and DPO ligands in U-DPO-10 are shown as red and sky blue, respectively).

Structural Diversity of Uranyl-DPO Compounds Related to Varying Conditions. As discussed above, a total of ten DPO-involved uranyl compounds, ranging from U-DPO-

https://doi.org/10.1021/acsomega.3c00640
ACS Omega 2023, 8, 8894−8909

1 to U-DPO-10 with diversity in structures, were synthesized here under different conditions (Figure 11 and Table S2). In these compounds, different kinds of coordination spheres of uranyl could be observed, including those coordinated only by DPO ligands, coordinated by DPO ligands together with oxyanions, hydroxyl ion, or water molecules, or coordinated by DPO ligands together with carboxyl ligands. It can be seen that the coordination of uranyl by DPO, together with other O-donors, plays a crucial role. As for DPO, it is interesting that this ditopic ligand shows three different coordination modes (Figure S7) including the most observed biconnected linker and another two exceptions (i.e., DPO without uranyl coordination in U-DPO-1 and monodentate DPO in U-DPO-3). Indeed, coordination behaviors of DPO ligands with uranyl centers in these uranyl compounds are largely affected by the presence or absence of other O-donors including solvent molecules, anions, and carboxylate ligands added during the formation of uranyl-DPO compounds. Meanwhile, other factors such as reaction temperature and solution acidity also have an indirect effect on the formation of uranyl-DPO compounds though promoting uranyl hydrolysis and reducing the coordination capacity of O-donors. A comprehensive discussion on the syntheses of these uranyl compounds, especially on coordination behaviors of DPO ligands among them, are discussed in detail as follows.

As a starting point, U-DPO-1, U-DPO-2, and U-DPO-3 are synthesized in aqueous solution using uranyl nitrate as the uranyl source. Due to the involvement of nitrate and water, there is competitive coordination of DPO with nitrate and water molecules toward uranyl ion, which can be effectively regulated by different reaction conditions. For instance, although both U-DPO-1 and U-DPO-2 were obtained by evaporation at room temperature, the former was synthesized at lower initial pH while the latter was at higher pH. Although there is no deprotonation process for DPO ligands, low acidity is unfavorable for the competitive coordination between DPO ligands and water molecules for uranyl. Therefore, unlike the separated structures of DPO and uranyl nitrate in U-DPO-1, the ditopic DPO ligands in U-DPO-2 coordinate directly with uranyl cation to a 1D chain structure, through nitrate ions still present in the coordination sphere of uranyl center. Moreover, U-DPO-3 is obtained under hydrothermal conditions with the same ratio of DPO to uranyl cations as U-DPO-1 and U-DPO-2. When comparing U-DPO-3 with U-DPO-1 and U-DPO-2, it can be seen that the increase of reaction temperature promotes the hydrolysis of uranyl ion, thus resulting in the formation of a final 1D polymeric uranyl chain.

In order to avoid competitive coordination from nitrate and water, another uranyl source $UO_2(CF_3SO_3)_2$ is employed, and due to the hydrophobicity of $UO_2(CF_3SO_3)_2$, an organic solvent CH_3CN is used to prepare the stock solution of $UO_2(CF_3SO_3)_2$ and serves as the reaction medium for solvothermal assembly.[75] As a result, three uranyl coordination polymers with 2D and 3D cationic skeletons ranging from U-DPO-4 to U-DPO-6 were obtained. In these $CF_3SO_3^-$-involved uranyl compounds, the uranyl centers are all five-coordinated on the equatorial plane, but there are minor variations in ligand types and numbers. Specifically, four DPO molecules and a $CF_3SO_3^-$ anion are included in U-DPO-4, four DPO ligands and one H_2O molecule are in U-DPO-5, and all five DPO ligands are in U-DPO-6. The results show that using a uranyl source $UO_2(CF_3SO_3)_2$ with weakly coordinating $CF_3SO_3^-$ anion dissolved in the organic solvent CH_3CN significantly increases the engagement of DPO ligands in the uranyl coordination sphere (4−5 DPO ligands for each uranyl), though the $CF_3SO_3^-$ ions and water molecule also participate in coordination with a uranyl center in U-DPO-4 and U-DPO-5. Beneficial to the feature of monodentate coordination, DPO shows the high degree of engagement in a uranyl coordination environment to achieve coordination saturation of the uranyl center. As a consequence, the space around the equatorial plane of uranyl becomes crowded. In order to reduce the possible steric hindrance of these co-occurring DPO molecules, two rigid pyridine rings have to rotate out and keep away from each other by adjusting their spatial orientation and dihedral angles with other adjacent DPO ligands. Along this line, high connectivity of the uranyl node and variable spatial orientation of DPO linkers lead to the formation of uranyl coordination polymers with higher dimensionality as exemplified by 2D networks observed in U-DPO-4 and 3D frameworks in U-DPO-5 and U-DPO-6.

Moreover, three aromatic or alkyl dicarboxylic acids, i.e., terephthalic acid (H_2TPA), isophthalic acid (H_2IPA), and succinic acid (H_2SA), are employed as auxiliary ligands to synthesize mixed-ligand uranyl compounds. Four uranyl compounds, including uranyl compounds from U-DPO-7 to U-DPO-10, have been obtained. Interestingly, DPO ligands show good compatibility with these carboxylate linkers, both of them being involved in the final uranyl compounds serving as two complementary components. It can be seen that aromatic carboxylate linker TPA^{2-} and IPA^{2-} with better rigidity and comparable size to DPO ligands are easier to form 2D network structures together with DPO. On the other hand, the SA^{2-} linker with a flexible aliphatic backbone easily changes its conformation in space and thus leads to more structural variation of the resultant uranyl compounds. Specifically, the evaporation method produces U-DPO-9 with a monomeric uranyl-linked 2D network similar to that of U-DPO-7, while the hydrothermal reaction gives the product of U-DPO-10 with a final 3D framework based on a monohydroxyl-bridging dimeric uranyl node. Again, a comparison between U-DPO-9 and U-DPO-10 shows that elevated pH, together with increasing temperature, facilitates the hydrolysis of uranyl and subsequently promotes the formation of uranyl compounds with more complex structure.

A Comparison of Bonding Nature between Different Kinds of U−O Bonds. As a kind of N-oxide group with typical Lewis basicity,[76] DPO shows good uranyl coordination ability in uranyl-DPO compounds discussed above. Meanwhile, the comparison between this series of uranyl-DPO compounds from U-DPO-1 to U-DPO-10 demonstrates the possible competitive coordination between different O-donors in the reaction system. In order to quantitatively figure out the bonding strength of different oxygen donors with uranium, theoretical analyses using DFT calculations are conducted on several simplified models of uranyl-DPO compounds including representative U−O bonds of interest.

The bond distance and bond orders including Wiberg (WBO),[77] Gophinathan−Jug (GJBO),[78] and Nalewajski−Mrozek bond orders (NMBO)[79] of the associated U−O bonds from optimized models of selected uranyl UPO compounds were shown in Table 3. All these three kinds of bond orders follow the trend of $U{\equiv}O_{ax}$ < U−O(η^2-COO^-) < U−O(DPO) < U−O(NO_3^-, H_2O, $CF_3SO_3^-$, and η^1-COO^-). For example, the WBO bond orders of U−O(DPO) bonds are within the range of 0.559−0.605, which are generally larger than that of U−O(H_2O) (0.348). Compared to anionic donors like nitrate and triflate, the bond affinity of DPO with uranium is also

https://doi.org/10.1021/acsomega.3c00640
ACS Omega 2023, 8, 8894−8909

Table 3. Bond Distances Including U−O(DPO), U−O(H_2O), U−O($CF_3SO_3^-$), U−O(COO^-), and U−O(Axial) Bonds (Å) in Simplified Models That Are Extracted from Representative Crystal Structures of U-DPO-2, U-DPO-4, U-DPO-5, U-DPO-7, and U-DPO-9 and Optimized by DFT and the Corresponding Bond Orders at the BP86/ZORA/TZ2P Level of Theory

compound	bond type	optimized distance	WBO	GJBO	NMBO
U-DPO-2	U≡O_{ax}	1.765	2.113	2.368	2.710
	U−O(DPO)	2.361	0.590	0.600	0.789
	U−O(NO_3^-)	2.541	0.398	0.389	0.500
U-DPO-4	U≡O_{ax}	1.768	2.073	2.320	2.669
	U−O(DPO)	2.367	0.570	0.545	0.662
	U−O(SO_3^-)	2.408	0.443	0.478	0.584
U-DPO-5	U≡O_{ax}	1.758	2.090	2.330	2.677
	U−O(DPO)	2.339	0.605	0.621	0.816
	U−O(H_2O)	2.431	0.348	0.362	0.514
U-DPO-7	U≡O_{ax}	1.770	2.130	2.370	2.705
	U−O(DPO)	2.387	0.559	0.561	0.737
	U−O(η^2-COO^-)	2.517	0.387	0.397	0.509
U-DPO-9	U≡O_{ax}	1.765	2.108	2.356	2.700
	U−O(DPO)	2.360	0.572	0.588	0.775
	U−O(η^1-COO^-)	2.305	0.626	0.682	0.853
	U−O(η^2-COO^-)	2.456	0.416	0.431	0.551

stronger, as exemplified by the WBO bond orders of U−O(NO_3^-) (0.398) or U−O(SO_3^-) (0.443). Moreover, the U−O(DPO) bond is comparable to the anionic carboxylate group, where the bond affinity of DPO with uranium is slightly weaker than that of η^1-COO^- (0.626) but significantly stronger than that of η^2-COO^- (0.387, 0.416). The DFT analysis of bond orders of different U−O bonds here shows that, as an aprotic oxygen donor, DPO exhibits good binding ability to the uranium metal center, which should be the underlying driving force to achieve competition or cooperation between DPO and other anionic ligands, just as we have seen in those uranyl DPO compounds.

Meanwhile, the Electron Localization Function (ELF) diagrams located on the equatorial planes of the uranyl ion are shown in Figure 12. It is found that the electron density is mainly located near the coordinating oxygen atoms, which is consistent

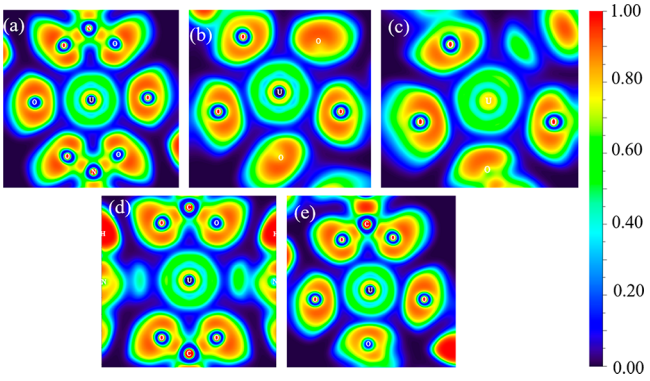

Figure 12. ELF diagrams for the equatorial plane of uranyl for simplified models from U-DPO-2 (a), U-DPO-4 (b), U-DPO-5 (c), U-DPO-7 (d), and U-DPO-9 (e).

with the fact that oxygen atoms serve as good electron donors of uranium. Indeed, the electron donating ability of these oxygen-donor ligands are all good enough that no obvious difference between them is observed here. The topological analysis of electron density for the U−O bonds has been also explored by means of QTAIM analysis, and the related parameters including electronic density (ρ), Laplacian of electron density ($\nabla^2\rho$), energy density (H) and delocalization index (DI)[80] are shown in Table S2. Generally, $\rho > 0.20$ au and $\nabla^2\rho < 0$ au at the BCPs are the conditions of typical covalent bonds, while $\rho < 0.10$ au and $\nabla^2\rho > 0$ au at the BCPs indicate an ionic bond. The U≡O_{ax} bonds have obvious characteristic of covalent bonds, while the U−O(DPO) and U−O(NO_3^-, H_2O, $CF_3SO_3^-$, and COO^-) bonds are mainly ionic interactions. For all the U-DPO compounds, the ρ values of U−O(DPO) are larger than the U−O(NO_3^-, H_2O, $CF_3SO_3^-$, and η^2-COO^-) bonds (as mentioned above), which provides more evidence that the bond strength of U−O(DPO) is stronger than U−O(NO_3^-, H_2O, $CF_3SO_3^-$, and η^2-COO^-) bonds. Meanwhile, the DI value that represents the number of electron pairs shared between two atoms is also calculated. Again, the DI values of U−O(DPO) are larger than the U−O(NO_3^-, H_2O, $CF_3SO_3^-$, and η^2-COO^-) bonds, which suggest stronger delocalization and sharing of electrons in U−O(DPO) bonds.

Characterization of Physicochemical Properties. In all these ten uranyl-DPO compounds, only those that can be isolated in high phase purity, U-DPO-7 (Figure S8) and U-DPO-10 (Figure S9), are subject to subsequent physicochemical characterization including infrared spectroscopy (IR), thermogravimetric analysis (TGA), and photoluminescence (PL) spectra.

In IR spectra of U-DPO-7 and U-DPO-10 (Figure S10), the absorption peaks near 918 cm^{-1} for U-DPO-7 and 914 cm^{-1} for U-DPO-10 confirm the presence of the uranyl cation with the asymmetric stretching. Vibration peaks around 1687 cm^{-1} in U-DPO-7 and 1656 cm^{-1} in U-DPO-10 are assigned to the vibrations of carboxyl groups in these two compounds. Furthermore, the shift of vibrations resulting from the N−O bond (1240 cm^{-1} in DPO ligand vs 1215 cm^{-1} in U-DPO-7 and U-DPO-10) before and after uranyl coordination are also observed. TGA analyses of U-DPO-7 and U-DPO-10 (Figure S11) demonstrate their good thermal stability. For U-DPO-7, two obvious weight losses in the whole temperature range of 30−800 °C can be observed. The first weight loss within 230−280 °C can be ascribed to the loss of solvent water molecules filling in the lattice channel. Following this weight loss, the integral framework of U-DPO-7 begins to collapse at 380 °C. U-DPO-10 is more thermally stable than U-DPO-7 with only one sharp weight loss at ∼350 °C that might correspond to the onset temperature of framework collapse.

In the photoluminescence spectrum (Figure 13), U-DPO-10 shows a characteristic emission similar to that of uranyl nitrate but with a minor red shift. Nevertheless, the fluorescent emission of U-DPO-7 affords a broad peak, resembling the phenomenon observed for $[(UO_2)_2(OH)(DPO)_2][Ir(CN)_6]\cdot nH_2O$ reported previously by Chorazy et al.[57] A recent work by Thuéry et al.[81] attributes this broad emission to strong uranyl−uranyl interactions within the hydroxo-/oxo-bridged clusters, but this mechanism could not be applied in U-DPO-7 that has only monomeric uranyl node, let alone U-DPO-10 with a dimeric uranyl unit but exhibiting typical luminescence characteristics of uranyl. Considering the light-absorbing nature of the aromatic TPA^{2-} ligand anchored to the uranyl center, the

https://doi.org/10.1021/acsomega.3c00640
ACS Omega 2023, 8, 8894−8909

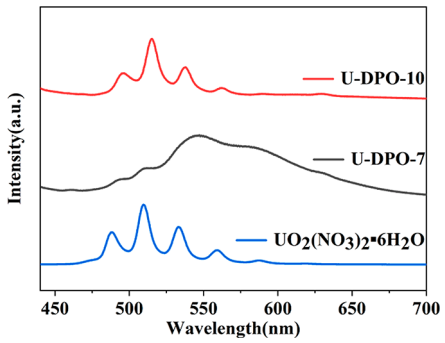

Figure 13. Solid-state luminescence emission spectra of U-DPO-7 and U-DPO-10 with $UO_2(NO_3)_2{\cdot}6H_2O$ as control.

occurrence of this kind of broad peak should be originated from the interaction between uranyl and the two TPA^{2-} linkers in its coordination sphere, which diminishes the characteristic "five-finger" emission peaks of the uranyl node in U-DPO-7. Such interference stemming from aromatic TPA ligand is also reported in other uranyl-TPA compounds.[82]

CONCLUSIONS

Under different reaction conditions using varying uranyl sources and/or auxiliary ligand, the N-oxide ligand DPO featuring an aprotic nature was used to construct uranyl compounds, and ten DPO-involved uranyl compounds, U-DPO-1 to U-DPO-10, have been successful. In U-DPO-1 to U-DPO-3, the participation of anionic nitrate or a hydroxyl group affects the coordination mode of DPO to uranyl, and three different kinds of coordination modes (i.e., uncoordinated, monodentate, and biconnected) are observed. Crystal structures of U-DPO-4 to U-DPO-6 obtained from $UO_2(CF_3SO_3)_2$ in acetonitrile precludes the participation of nitrate and hydroxyl and helps to increase the engagement of DPO ligands (a total of 4−5 DPO ligands for each uranyl) in the uranyl coordination sphere. Among U-DPO-7 to U-DPO-10, the DPO ligand can collaborate well with carboxylic acids such as H_2TPA, H_2IPA, and H_2SA to generate final mixed-ligand uranyl compounds. Analysis of the bonding nature of U−O with different donors by theoretical calculation reveals that the bonding strength of DPO is better than that of anionic $CF_3SO_3^-$, nitrate, or a neutral H_2O molecule and comparable to the anionic carboxylate group in η^1-mode, which supports the above observation about the uranyl coordination ability of DPO in these uranyl-DPO compounds. This work provides good potential of DPO to construct uranyl compounds and will impel more studies on the exploration of new actinide compounds based on such kinds of aprotic N-oxide-typed O-donors. Meanwhile, for the construction of functional actinide materials, the combination of this kind of O-donor with other anionic linkers is also worth looking forward to.

ASSOCIATED CONTENT

Supporting Information

The Supporting Information is available free of charge at https://pubs.acs.org/doi/10.1021/acsomega.3c00640.

Synthesis and characterization for DPO and ten uranyl-DPO compounds from U-DPO-1 to U-DPO-10; PXRD, IR, and TGA data for U-DPO-7 and U-DPO-10; selected bond lengths and calculations (PDF)

Crystal data for all ten compounds (ZIP)

AUTHOR INFORMATION

Corresponding Authors

Meng Zhang − *Fundamental Science on Nuclear Safety and Simulation Technology Laboratory, College of Nuclear Science and Technology, Harbin Engineering University, Harbin 150001, China;* orcid.org/0000-0001-8065-8643; Email: zhangmeng1980@hrbeu.edu.cn

Lei Mei − *Laboratory of Nuclear Energy Chemistry, Institute of High Energy Physics, Chinese Academy of Sciences, Beijing 100049, China;* orcid.org/0000-0002-2926-7265; Email: meil@ihep.ac.cn

Authors

Jing-yang Wang − *Fundamental Science on Nuclear Safety and Simulation Technology Laboratory, College of Nuclear Science and Technology, Harbin Engineering University, Harbin 150001, China; Laboratory of Nuclear Energy Chemistry, Institute of High Energy Physics, Chinese Academy of Sciences, Beijing 100049, China*

Yang Liu − *Laboratory of Nuclear Energy Chemistry, Institute of High Energy Physics, Chinese Academy of Sciences, Beijing 100049, China*

Qiu-yan Jin − *Laboratory of Nuclear Energy Chemistry, Institute of High Energy Physics, Chinese Academy of Sciences, Beijing 100049, China; University of Chinese Academy of Sciences, Beijing 100049, China*

Kong-qiu Hu − *Laboratory of Nuclear Energy Chemistry, Institute of High Energy Physics, Chinese Academy of Sciences, Beijing 100049, China*

Ji-pan Yu − *Laboratory of Nuclear Energy Chemistry, Institute of High Energy Physics, Chinese Academy of Sciences, Beijing 100049, China*

Cai-shan Jiao − *Fundamental Science on Nuclear Safety and Simulation Technology Laboratory, College of Nuclear Science and Technology, Harbin Engineering University, Harbin 150001, China*

Wei-qun Shi − *Laboratory of Nuclear Energy Chemistry, Institute of High Energy Physics, Chinese Academy of Sciences, Beijing 100049, China;* orcid.org/0000-0001-9929-9732

Complete contact information is available at: https://pubs.acs.org/10.1021/acsomega.3c00640

Notes

The authors declare no competing financial interest.

ACKNOWLEDGMENTS

This work is financially supported by the National Natural Science Foundation of China (22122609, 22076186, U2267223, and 22076187), the Fundamental Research Funds for the Central Universities (No. 3072022JC1501) and the National Science Fund for Distinguished Young Scholars (21925603). The Youth Innovation Promotion Association of CAS (2020014) is also acknowledged.

REFERENCES

(1) Kitagawa, S.; Kitaura, R.; Noro, S. Functional porous coordination polymers. *Angew. Chem., Int. Ed.* **2004**, *43* (18), 2334−2375.

(2) Janiak, C. Engineering coordination polymers towards applications. *Dalton Trans.* **2003**, No. 14, 2781−2804.

(3) Cook, T. R.; Zheng, Y.-R.; Stang, P. J. Metal-Organic Frameworks and Self-Assembled Supramolecular Coordination Complexes: Comparing and Contrasting the Design, Synthesis, and Functionality of Metal-Organic Materials. *Chem. Rev.* **2013**, *113* (1), 734−777.

(4) Snelgrove, M. P.; Hardie, M. J. Coordination polymers with embedded recognition sites: lessons from cyclotriveratrylene-type ligands. *CrystEngComm* **2021**, *23* (23), 4087−4102.
(5) Tranchemontagne, D. J.; Mendoza-Cortes, J. L.; O'Keeffe, M.; Yaghi, O. M. Secondary building units, nets and bonding in the chemistry of metal-organic frameworks. *Chem. Soc. Rev.* **2009**, *38* (5), 1257−1283.
(6) Han, Y.; Li, J.-R.; Xie, Y.; Guo, G. Substitution reactions in metal-organic frameworks and metal-organic polyhedra. *Chem. Soc. Rev.* **2014**, *43* (16), 5952−5981.
(7) Zeng, X.; Nyquist, Y.; Zhang, Q.; Hans-JürgenButt; Wu, S. Light-induced assembly of colloidal nanoparticles based on photo-controlled metal−ligand coordination. *Supramol. Mater.* **2022**, *1*, 100004−100008.
(8) Yang, F.; Xu, G.; Dou, Y.; Wang, B.; Zhang, H.; Wu, H.; Zhou, W.; Li, J.-R.; Chen, B. A Flexible Metal-Organic Framework With a High Density of Sulfonic Acid Sites for Proton Conduction. *Nature Energy* **2017**, *2* (11), 877−883.
(9) Hu, K.-Q.; Wu, Q.-Y.; Mei, L.; Zhang, X.-L.; Ma, L.; Song, G.; Chen, D.-Y.; Wang, Y.-T.; Chai, Z.-F.; Shi, W.-Q. Novel Viologen Derivative Based Uranyl Coordination Polymers Featuring Photochromic Behaviors. *Chem.—Eur. J.* **2017**, *23* (71), 18074−18083.
(10) Kong, X. H.; Hu, K. Q.; Mei, L.; Li, A.; Liu, K.; Zeng, L. W.; Wu, Q. Y.; Chai, Z. F.; Nie, C. M.; Shi, W. Q. Double-Layer Nitrogen-Rich Two-Dimensional Anionic Uranyl-Organic Framework for Cation Dye Capture and Catalytic Fixation of Carbon Dioxide. *Inorg. Chem.* **2021**, *60* (15), 11485−11495.
(11) Haque, E.; Jun, J. W.; Jhung, S. H. Adsorptive removal of methyl orange and methylene blue from aqueous solution with a metal-organic framework material, iron terephthalate (MOF-235). *J. Hazard. Mater.* **2011**, *185* (1), 507−511.
(12) Haque, E.; Lee, J. E.; Jang, I. T.; Hwang, Y. K.; Chang, J. S.; Jegal, J.; Jhung, S. H. Adsorptive removal of methyl orange from aqueous solution with metal-organic frameworks, porous chromium-benzenedicarboxylates. *J. Hazard. Mater.* **2010**, *181* (1−3), 535−542.
(13) Baruah, J. B. Coordination polymers in adsorptive remediation of environmental contaminants. *Coord. Chem. Rev.* **2022**, *470*, 214694.
(14) Huang, Z. W.; Hu, K. Q.; Mei, L.; Wang, C. Z.; Chen, Y. M.; Wu, W. S.; Chai, Z. F.; Shi, W. Q. Potassium Ions Induced Framework Interpenetration for Enhancing the Stability of Uranium-Based Porphyrin MOF with Visible-Light-Driven Photocatalytic Activity. *Inorg. Chem.* **2021**, *60* (2), 651−660.
(15) Chughtai, A. H.; Ahmad, N.; Younus, H. A.; Laypkov, A.; Verpoort, F. Metal-organic frameworks: versatile heterogeneous catalysts for efficient catalytic organic transformations. *Chem. Soc. Rev.* **2015**, *44* (19), 6804−6849.
(16) Huang, N.; Wang, K.; Drake, H.; Cai, P.; Pang, J.; Li, J.; Che, S.; Huang, L.; Wang, Q.; Zhou, H.-C. Tailor-Made Pyrazolide-Based Metal-Organic Frameworks for Selective Catalysis. *J. Am. Chem. Soc.* **2018**, *140* (20), 6383−6390.
(17) Liu, Y.; Du, P.; Teng, Q.; Sun, H.; Ye, X.; Wang, Z. Self-assembly of fibril-forming histidine-rich peptides for cofactor-free oxidase-mimetic catalysis. *Supramol. Mater.* **2022**, *1*, 100012−100017.
(18) Ai, J.; Chen, F.-Y.; Gao, C.-Y.; Tian, H.-R.; Pan, Q.-J.; Sun, Z.-M. Porous Anionic Uranyl-Organic Networks for Highly Efficient Cs+ Adsorption and Investigation of the Mechanism. *Inorg. Chem.* **2018**, *57* (8), 4419−4426.
(19) Zeng, L.-W.; Hu, K.-Q.; Mei, L.; Li, F.-Z.; Huang, Z.-W.; An, S.-W.; Chai, Z.-F.; Shi, W.-Q. Structural Diversity of Bipyridinium-Based Uranyl Coordination Polymers: Synthesis, Characterization, and Ion-Exchange Application. *Inorg. Chem.* **2019**, *58* (20), 14075−14084.
(20) Mei, L.; Li, F.-z.; Lan, J.-h.; Wang, C.-z.; Xu, C.; Deng, H.; Wu, Q.-y.; Hu, K.-q.; Wang, L.; Chai, Z.-f.; Chen, J.; Gibson, J. K.; Shi, W.-q. Anion-adaptive crystalline cationic material for (TcO4-)-Tc-99 trapping. *Nat. Commun.* **2019**, *10*, 1532−1543.
(21) Yuan, L. Y.; Tian, M.; Lan, J. H.; Cao, X. Z.; Wang, X. L.; Chai, Z. F.; Gibson, J. K.; Shi, W. Q. Defect engineering in metal-organic frameworks: a new strategy to develop applicable actinide sorbents. *Chem. Commun.* **2018**, *54* (4), 370−373.
(22) Liu, C.-X.; Liang, N. Zn-Based Metal-Organic Framework: Luminescence Sensing for the Detection of Fe^{3+} Ions and Treatment Activity on Child Allergic Purpura. *J. Solid State Chem.* **2021**, *303*, 122483−122488.
(23) Whelan, É.; Steuber, F. W.; Gunnlaugsson, T.; Schmitt, W. Tuning Photoactive Metal−Organic Frameworks for Luminescence and Photocatalytic Applications. *Coord. Chem. Rev.* **2021**, *437*, 213757.
(24) Cornelio, J.; Zhou, T. Y.; Alkas, A.; Telfer, S. G. Systematic Tuning of the Luminescence Output of Multicomponent Metal-Organic Frameworks. *J. Am. Chem. Soc.* **2018**, *140* (45), 15470−15476.
(25) Bunzli, J. C. G. Review: Lanthanide coordination chemistry: from old concepts to coordination polymers. *J. Coord. Chem.* **2014**, *67* (23−24), 3706−3733.
(26) Li, B.; Wen, H. M.; Cui, Y. J.; Qian, G. D.; Chen, B. L. Multifunctional lanthanide coordination polymers. *Prog. Polym. Sci.* **2015**, *48*, 40−84.
(27) Moulton, B.; Zaworotko, M. J. Coordination polymers: toward functional transition metal sustained materials and supermolecules. *Curr. Opin. Solid State Mater. Sci.* **2002**, *6* (2), 117−123.
(28) Burns, P. C.; Ewing, R. C.; Navrotsky, A. Nuclear Fuel in a Reactor Accident. *Science* **2012**, *335* (6073), 1184−1188.
(29) Dam, H. H.; Reinhoudt, D. N.; Verboom, W. Multicoordinate ligands for actinide/lanthanide separations. *Chem. Soc. Rev.* **2007**, *36* (2), 367−377.
(30) Lv, K.; Fichter, S.; Gu, M.; Marz, J.; Schmidt, M. An updated status and trends in actinide metal-organic frameworks (An-MOFs): From synthesis to application. *Coord. Chem. Rev.* **2021**, *446*, 214011.
(31) Su, J.; Chen, J. S. MOFs of Uranium and the Actinides. In *Lanthanide Metal-Organic Frameworks*; Cheng, P., Ed.; Springer, 2014; Vol. *163*, pp 265−295;.
(32) Knope, K. E.; Soderholm, L. Solution and Solid-state Structural Chemistry of Actinide Hydrates and Their Hydrolysis and Condensation Products. *Chem. Rev.* **2013**, *113*, 944−994.
(33) Moore, K. T.; van der Laan, G. Nature of the 5f states in actinide metals. *Rev. Mod. Phys.* **2009**, *81* (1), 235−298.
(34) Szabo, Z.; Toraishi, T.; Vallet, V.; Grenthe, I. Solution Coordination Chemistry of Actinides: Thermodynamics, Structure and Reaction Mechanisms. *Coord. Chem. Rev.* **2006**, *250*, 784−815.
(35) Burns, P. C.; Ewing, R. C.; Hawthorne, F. C. The crystal chemistry of hexavalent uranium: Polyhedron geometries, bond-valence parameters, and polymerization of polyhedra. *Can. Mineral.* **1997**, *35*, 1551−1570.
(36) Maher, K.; Bargar, J. R.; Brown, J. G. E. Environmental Speciation of Actinides. *Inorg. Chem.* **2013**, *52*, 3510−3532.
(37) Andrews, M. B.; Cahill, C. L. Uranyl Bearing Hybrid Materials: Synthesis, Speciation, and Solid-State Structures. *Chem. Rev.* **2013**, *113* (2), 1121−1136.
(38) Wang, K.-X.; Chen, J.-S. Extended Structures and Physicochemical Properties of Uranyl-Organic Compounds. *Acc. Chem. Res.* **2011**, *44* (7), 531−540.
(39) Loiseau, T.; Mihalcea, I.; Henry, N.; Volkringer, C. The Crystal Chemistry of Uranium Carboxylates. *Coord. Chem. Rev.* **2014**, *266*, 69−109.
(40) Thuery, P.; Harrowfield, J. Recent advances in structural studies of heterometallic uranyl-containing coordination polymers and polynuclear closed species. *Dalton Trans.* **2017**, *46* (40), 13660−13667.
(41) Yang, W. T.; Parker, T. G.; Sun, Z. M. Structural chemistry of uranium phosphonates. *Coord. Chem. Rev.* **2015**, *303*, 86−109.
(42) Mei, L.; Shi, W.-q.; Chai, Z.-f. Ordered Entanglement in Actinide-Organic Coordination Polymers. *Bull. Chem. Soc. Jpn.* **2018**, *91* (4), 554−562.
(43) Li, F. Z.; Geng, J. S.; Hu, K. Q.; Yu, J. P.; Liu, N.; Chai, Z. F.; Mei, L.; Shi, W. Q. Proximity Effect in Uranyl Coordination of the Cucurbit[6]urilBipyridinium Pseudorotaxane Ligand for Promoting Host−Guest Synergistic Chelating. *Inorg. Chem.* **2021**, *60*, 10522−10534.
(44) Wang, J. Y.; Mei, L.; Huang, Z. W.; Chi, X. W.; Geng, J. S.; Hu, K. Q.; Yu, J. P.; Jiao, C. S.; Zhang, M.; Chai, Z. F.; Shi, W. Q. Coordination-

https://doi.org/10.1021/acsomega.3c00640
ACS Omega 2023, 8, 8894−8909

Adaptive Polydentate Pseudorotaxane Ligand for Capturing Multiple Uranyl Species. *Inorg. Chem.* **2022**, *61* (7), 3058−3071.
(45) Lv, K.; Urbank, C.; Patzschke, M.; Marz, J.; Kaden, P.; Weiss, S.; Schmidt, M. MOFs with 12-Coordinate 5f-Block Metal Centers. *J. Am. Chem. Soc.* **2022**, *144* (7), 2879−2884.
(46) Gilson, S. E.; Fairley, M.; Hanna, S. L.; Szymanowski, J. E. S.; Julien, P.; Chen, Z. J.; Farha, O. K.; LaVerne, J. A.; Burns, P. C. Unusual Metal-Organic Framework Topology and Radiation Resistance through Neptunyl Coordination Chemistry. *J. Am. Chem. Soc.* **2021**, *143* (42), 17354−17359.
(47) Mei, L.; Ren, P.; Wu, Q. Y.; Ke, Y. B.; Geng, J. S.; Liu, K.; Xing, X. Q.; Huang, Z. W.; Hu, K. Q.; Liu, Y. L.; Yuan, L. Y.; Mo, G.; Wu, Z. H.; Gibson, J. K.; Chai, Z. F.; Shi, W. Q. Actinide Separation Inspired by Self-Assembled Metal-Polyphenolic Nanocages. *J. Am. Chem. Soc.* **2020**, *142* (39), 16538−16545.
(48) Andreo, J.; Priola, E.; Alberto, G.; Benzi, P.; Marabello, D.; Proserpio, D. M.; Lamberti, C.; Diana, E. Autoluminescent Metal-Organic Frameworks (MOFs): Self-Photoemission of a Highly Stable Thorium MOF. *J. Am. Chem. Soc.* **2018**, *140* (43), 14144−14149.
(49) Sasaki, Y.; Sugo, Y.; Suzuki, S.; Tachimori, S. The novel extractants, diglycolamides, for the extraction of lanthanides and actinides in HNO3-n-dodecane system. *Solvent Extr. Ion Exch.* **2001**, *19* (1), 91−103.
(50) Ansari, S. A.; Pathak, P.; Mohapatra, P. K.; Manchanda, V. K. Chemistry of Diglycolamides: Promising Extractants for Actinide Partitioning. *Chem. Rev.* **2012**, *112* (3), 1751−1772.
(51) Beltrami, D.; Cote, G.; Mokhtari, H.; Courtaud, B.; Moyer, B. A.; Chagnest, A. Recovery of Uranium from Wet Phosphoric Acid by Solvent Extraction Processes. *Chem. Rev.* **2014**, *114* (24), 12002−12023.
(52) Dolgopolova, E. A.; Ejegbaywo, O. A.; Martin, C. R.; Smith, M. D.; Setyawan, W.; Karakalos, S. G.; Henager, C. H.; zur Loye, H.-C.; Shustova, N. B. Multifaceted Modularity: A Key for Stepwise Building of Hierarchical Complexity in Actinide Metal-Organic Frameworks. *J. Am. Chem. Soc.* **2017**, *139* (46), 16852−16861.
(53) Mei, L.; Wu, Q. Y.; An, S. W.; Gao, Z. Q.; Chai, Z. F.; Shi, W. Q. Silver Ion-Mediated Heterometallic Three-Fold Interpenetrating Uranyl-Organic Framework. *Inorg. Chem.* **2015**, *54*, 10934−10945.
(54) Weng, Z. H.; Zhang, Z. H.; Olds, T.; Sterniczuk, M.; Burns, P. C. Copper(I) and Copper(II) Uranyl Heterometallic Hybrid Materials. *Inorg. Chem.* **2014**, *53*, 7993−7998.
(55) Kerr, A. T.; Cahill, C. L. Postsynthetic Rearrangement/Metalation as a Route to Bimetallic Uranyl Coordination Polymers Syntheses, Structures, and Luminescence. *Cryst. Growth Des.* **2014**, *14*, 1914−1921.
(56) Meng, L.; Liang, Y. Y.; Mei, L.; Geng, J. S.; Hu, K. Q.; Yu, J. P.; Wang, X. P.; Fujita, T.; Chai, Z. F.; Shi, W. Q. Mixed-Ligand Uranyl Squarate Coordination Polymers: Structure Regulation and Redox Activity. *Inorg. Chem.* **2022**, *61* (1), 302−316.
(57) Chorazy, S.; Zakrzewski, J. J.; Reczynski, M.; Sieklucka, B. Multicolour uranyl emission efficiently tuned by hexacyanidometallates within hybrid coordination frameworks. *Chem. Commun.* **2019**, *55* (21), 3057−3060.
(58) Zhang, C.; Guo, F. W.; Dai, Y.; Zhang, Y.; Feng, J.; Wang, N.; Wang, J. [(UO2)(C10H8N2O2)(2)][HPW12O40]: The First Case of a Uranyl Coordination Network Containing a Keggin-Type Polyoxometalate. *Eur. J. Inorg. Chem.* **2020**, *2020* (48), 4577−4580.
(59) Dai, Y.; Chai, H.-M.; Zhang, R.-X.; Min, J.-A.; Wang, Z.; Zhang, M.; Zhang, Y.; Feng, J.; Zhang, C.; Wang, J. A Series of Uranium-Organic Frameworks: Crucial Role of the Protonation Ability of Auxiliary Ligands. *Inorg. Chem. Commun.* **2020**, *111*, 107628.
(60) Jennifer, S. J.; Muthiah, P. T. Synthesis, crystal structure and spectroscopic studies of some organic/inorganic hybrid materials containing isostructural monomeric uranyl complexes bridged by bipyridyl typed ligands. *Inorg. Chim. Acta* **2014**, *416*, 69−75.
(61) Lyczko, K.; Lyczko, M.; Walo, M.; Lipkowski, J. Conversion of thorium(IV) oxide into thorium(IV) trifluoromethanesulfonate: Crystal structure of thorium(IV) trifluoromethanesulfonate dihydrate. *Inorg. Chem. Commun.* **2012**, *24*, 234−236.
(62) Aakeroy, C. B.; Epa, K.; Forbes, S.; Schultheiss, N.; Desper, J. Ranking relative hydrogen-bond strengths in hydroxybenzoic acids for crystal-engineering purposes. *Chem.—Eur. J.* **2013**, *19* (44), 14998−15003.
(63) Hoffart, D. J.; Habermehl, N. C.; Loeb, S. J. 4,4′-Bipyridine-N-monoxide. A hybrid ligand for building networks using a combination of metal-ligand and hydrogen-bonding interactions. *Dalton Trans.* **2007**, No. 27, 2870−2875.
(64) Sheldrick, G. M. SHELXT - Integrated space-group and crystal-structure determination. *Acta Crystallogr. A* **2015**, *71*, 3−8.
(65) Sheldrick, G. M. A short history of SHELX. *Acta Crystallogr. A* **2008**, *64* (1), 112−122.
(66) Te Velde, G. t.; Bickelhaupt, F. M.; Baerends, E. J.; Fonseca Guerra, C.; van Gisbergen, S. J.; Snijders, J. G.; Ziegler, T. Chemistry with ADF. *J. Comput. Chem.* **2001**, *22* (9), 931−967.
(67) Lenthe, E. v.; Baerends, E.-J.; Snijders, J. G. Relativistic regular two-component Hamiltonians. *J. Chem. Phys.* **1993**, *99* (6), 4597−4610.
(68) Bader, R. F. Bond Paths are not Chemical Bonds. *J. Phys. Chem. A* **2009**, *113* (38), 10391−10396.
(69) Savin, A.; Becke, A.; Flad, J.; Nesper, R.; Preuss, H.; Von Schnering, H. A new look at electron localization. *Angew. Chem., Int. Ed.* **1991**, *30* (4), 409−412.
(70) Savin, A.; Nesper, R.; Wengert, S.; Fässler, T. F. ELF: The Electron Localization Function. *Angew. Chem., Int. Ed.* **1997**, *36* (17), 1808−1832.
(71) Lu, T.; Chen, F. Multiwfn: a multifunctional wavefunction analyzer. *J. Comput. Chem.* **2012**, *33* (5), 580−592.
(72) Meng, L.; Liang, Y. Y.; Mei, L.; Geng, J. S.; Hu, K. Q.; Yu, J. P.; Wang, X. P.; Fujita, T.; Chai, Z. F.; Shi, W. Q. Mixed-Ligand Uranyl Squarate Coordination Polymers: Structure Regulation and Redox Activity. *Inorg. Chem.* **2022**, *61* (1), 302−316.
(73) Spackman, P. R.; Turner, M. J.; McKinnon, J. J.; Wolff, S. K.; Grimwood, D. J.; Jayatilaka, D.; Spackman, M. A. CrystalExplorer: a program for Hirshfeld surface analysis, visualization and quantitative analysis o molecular crystals. *J. Appl. Crystallogr.* **2021**, *54*, 1006−1011.
(74) Spackman, M. A.; Jayatilaka, D. Hirshfeld surface analysis. *CrystEngcomm* **2009**, *11* (1), 19−32.
(75) Hoffart, D. J.; Loeb, S. J. Metal-Organic Rotaxane Frameworks: Three-Dimensional Polyrotaxanes From Lanthanide-Ion Nodes, PyridiniumN-Oxide Axles, and Crown-Ether Wheels. *Angew. Chem., Int. Ed.* **2005**, *117*, 923−926.
(76) Lukomska, M.; Rybarczyk-Pirek, A. J.; Jablonski, M.; Palusiak, M. The nature of NO-bonding in N-oxide group. *Phys. Chem. Chem. Phys.* **2015**, *17* (25), 16375−16387.
(77) Wiberg, K. B. Application of the pople-santry-segal CNDO method to the cyclopropylcarbinyl and cyclobutyl cation and to bicyclobutane. *Tetrahedron* **1968**, *24* (3), 1083−1096.
(78) Gopinathan, M.; Jug, K. Valency. I. A quantum chemical definition and properties. *Theor. Chim. Acta* **1983**, *63* (6), 497−509.
(79) Nalewajski, R. F.; Mrozek, J.; Artur, M. Two-electron valence indices from the Kohn-Sham orbitals. *Int. J. Quantum Chem.* **1997**, *61* (3), 589−601.
(80) Fradera, X.; Austen, M. A.; Bader, R. F. The Lewis Model and Beyond. *J. Phys. Chem. A* **1999**, *103* (2), 304−314.
(81) Thuéry, P.; Atoini, Y.; Harrowfield, J. Isomerism in Benzenetricarboxylates: Variations in the Formation of Coordination Polymers with Uranyl Ion. *Cryst. Growth Des.* **2020**, *20* (11), 7368−7383.
(82) Mei, L.; Wang, C. Z.; Zhu, L. Z.; Gao, Z. Q.; Chai, Z. F.; Gibson, J. K.; Shi, W. Q. Exploring New Assembly Modes of Uranyl Terephthalate: Templated Syntheses and Structural Regulation of a Series of Rare 2D -> 3D Polycatenated Frameworks. *Inorg. Chem.* **2017**, *56* (14), 7694−7706.

https://doi.org/10.1021/acsomega.3c00640
ACS Omega 2023, 8, 8894−8909